LEVEL II

(12)

TELEDYNE MICRONETICS

7155 MISSION GORGE ROAD • P.O. BOX 20396 • SAN DIEGO, CALIFORNIA 92120
PHONE (714) 583-3525 • TWX 910-335-2085

TELEDYNE MICRONETICS
7155 Mission Gorge Road
San Diego, California 92120

(12)

(9) Final rept. Oct 79 – Mar 81,

(10) Lee H. Murphy
Steven Weisbrod

(14) REPORT R5-81

(11) MAR 81

(12) 71

(6) RCS MATRIX STUDIES OF SEA CLUTTER

FINAL REPORT

(15) Contract No. N00019-79-C-0625

Prepared for

Naval Air Systems Command
Washington, D. C. 20361

(15)

TABLE OF CONTENTS

		Page
1.0	INTRODUCTION	1
1.1	Objective of the Effort	1
1.2	Background Information	1
2.0	DESCRIPTION OF EXPERIMENTAL PROCEDURES	5
2.1	Site Geometry	5
2.2	Experimental Equipment	5
2.3	Calibration Procedures	9
3.0	PRELIMINARY EXPERIMENTAL RESULTS	19
3.1	Data Format	19
3.2	Target Data	22
3.3	RCS Matrix Measurements of Clutter	36
3.4	Clutter to Noise Ratio	53
3.5	Applicability to Target Classification	56
4.0	CONCLUSIONS AND RECOMMENDATIONS	57
	APPENDIX A	58

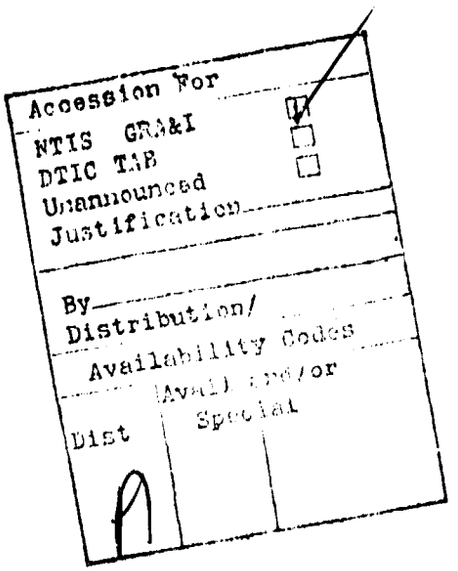

LIST OF FIGURES

Figure		Page
1	Foreground Terrain Profiles - Pt. Loma Site. . .	6
2	Incidence Angle on Sea Surface as Function of Range or Delay. Radar Height = 430'	7
3	General Site Topography.	11
4	Geometry of Specular and Non-specular Components of Reflection from a Dihedral.	17
5a	RCS Matrix Observation of a Sailboat	23
6a	RCS Matrix Observation of a Launch	27
7a	RCS Matrix Observation of a Sportfishing Boat. .	31
8a	RCS Matrix Observation of Sea Clutter at 2.9° Elevation Angle	37
9a	RCS Matrix Observation of Sea Clutter at 3.3° Elevation Angle	41
10a	RCS Matrix Observation of Sea Clutter at 4.1° Elevation Angle	45
11a	RCS Matrix Observation of Sea Clutter at 6.1° Elevation Angle	49
12	Clutter to Noise Ratio as a function of Range. .	54

LIST OF TABLES

Table I	RCS Matrix Radar Parameters.	10
Table II	Expected Clutter Values for Sea State 3.	55

SECURITY CLASSIFICATION OF THIS PAGE (When Data Entered)

REPORT DOCUMENTATION PAGE

READ INSTRUCTIONS BEFORE COMPLETING FORM

1. REPORT NUMBER	2. GOVT ACCESSION NO. AD-A099 191 / 3. RECIPIENT'S CATALOG NUMBER
4. TITLE (and Subtitle) RCS Matrix Studies of Sea Clutter	5. TYPE OF REPORT & PERIOD COVERED Final Report Oct 79 - Mar 81
	6. PERFORMING ORG. REPORT NUMBER
7. AUTHOR(s) L. A. Morgan S. Weisbrod	8. CONTRACT OR GRANT NUMBER(s) N00019-79-C-0625
9. PERFORMING ORGANIZATION NAME AND ADDRESS Teledyne Micronetics 7155 Mission Gorge Road San Diego, CA 92120	10. PROGRAM ELEMENT, PROJECT, TASK AREA & WORK UNIT NUMBERS
11. CONTROLLING OFFICE NAME AND ADDRESS Naval Air Systems Command Washington, D. C. 20361 Mr. J. W. Willis, Code AIR-310B	12. REPORT DATE March 1981
	13. NUMBER OF PAGES 64
14. MONITORING AGENCY NAME & ADDRESS(if different from Controlling Office)	15. SECURITY CLASS. (of this report) Unclassified
	15a. DECLASSIFICATION/DOWNGRADING SCHEDULE N/A

16. DISTRIBUTION STATEMENT (of this Report)

[redacted]

APPROVED FOR PUBLIC RELEASE;
DISTRIBUTION UNLIMITED

17. DISTRIBUTION STATEMENT (of the abstract entered in Block 20, if different from Report)

18. SUPPLEMENTARY NOTES

19. KEY WORDS (Continue on reverse side if necessary and identify by block number)

Polarization
Sea Clutter
RCS Matrix

20. ABSTRACT (Continue on reverse side if necessary and identify by block number)

The report describes the development of a mobile experimental facility for making observations of RCS matrix properties of sea clutter and of targets in sea clutter. The equipment is mounted in a van which was towed to a site on Pt. Loma at the NOSC facility in San Diego.

Preliminary measurements on clutter and targets of opportunity were taken and analyzed. The analysis confirms the salient features of sea clutter

DD FORM 1 JAN 73 1473 EDITION OF 1 NOV 65 IS OBSOLETE

SECURITY CLASSIFICATION OF THIS PAGE (When Data Entered)

properties deduced from the NRL Four Frequency Radar data collected some ten years ago. Experimental results also show that RCS matrix data is used in target signatures which should eventually lead to the development of an effective technique for target classification.

FOREWORD

This is the Final Report prepared by Teledyne Micronetics under Naval Air Systems Command Contract No. N00019-79-C-0625. The work reported here covers the period of time from October, 1979 through March, 1981. The work was administered by Mr. James W. Willis, Naval Air Systems Command, Code AIR-310B.

The project manager for Teledyne Micronetics was Dr. Steven Weisbrod. The other principal investigator was Mr. Lee A. Morgan.

We wish to acknowledge the assistance of Dr. Juergen Richter and Mr. Perry Snyder of Naval Ocean Systems Command in making the necessary arrangement for the preparations and utilization of the Point Loma site.

We are indebted to Mr. John C. Daley of NRL for his continuing cooperation in the development of theoretical models of sea clutter and targets.

We also wish to acknowledge many helpful comments and suggestions by Dr. Robert C. Hansen who was the NAVAIR consultant for this effort.

1.0 INTRODUCTION

1.1 Objective of the Effort

The immediate objective of the effort was to instrument an experimental capability to study RCS matrix of sea clutter and to collect some preliminary data from an experimental site at NOSC to confirm experimental results obtained with the NRL Four Frequency Radar data taken some ten years ago. The long term objective of this effort is to refine the NRL results and to quantify the RCS matrix technique potential to improve radar target detectability in sea clutter and to evaluate the applicability of this technique to target classification.

In order to make this report as much self-contained as possible, a brief overview will be given of the earlier studies and the basic concepts.

1.2 Background Information

During the past few years Teledyne Micronetics, under the sponsorship of NAVAIR, and also within the past two years under the sponsorships of NAVAIR and RADC, has been carrying out a series of studies aimed at the utilization of polarization signatures to augment conventional radar techniques in order to achieve improved target detectability and classification in the presence of clutter.

The initial efforts carried out under NAVAIR contracts were aimed at a systematic analysis of polarization signatures of sea clutter and sea clutter with targets. The study was motivated in part by the requirement to improving radar detectability of targets in sea clutter and in part by scattered reports in literature that occasionally significant improvement in target detectability was achieved by such techniques as using horizontally polarized signals for target illumination and vertically polarized signals for signal reception.

It was therefore felt that useful information could be gained if a systematic investigation were carried out on polarization properties of sea clutter to establish if indeed there exist some properties which are stable in a statistical sense over a period of time long in comparison with time on target and also if the presence of a target causes a significant change in these properties to allow identification of the radar return for the presence of a target with reasonably high degree of confidence and low probability of false alarm.

The results of these earlier studies have qualitatively demonstrated that polarization properties of sea clutter are statistically quite different from those of man-made targets and utilization of polarization signatures can effectively augment radar detectability of targets in sea clutter.

The experimental data which was used was the NRL Airborne Four Frequency Radar data which was taken by NRL in the late '60s and '70s. Radar operating at P, L, C, and X-band were sequentially switched using alternately vertical and horizontal polarizations. Returned scatter was measured on both polarizations simultaneously and relative amplitudes and phase were digitized and recorded on magnetic tape. As it turned out, only the cosine of the phase angle was actually available and a considerable amount of data processing was needed to identify the quadrant with a reasonable degree of confidence. It should be emphasized that this effort would have been completely impossible without the tremendous assistance and cooperation which we received from NRL.

Although there were some serious problems with the data which limited the quantitative aspects of the study, the qualitative results demonstrated beyond any reasonable doubt that sea clutter exhibits certain well-defined polarization characteristics which were demonstrated by studying various properties

of the RCS matrix. Furthermore, the NRL data also clearly demonstrated that these properties were significantly disturbed in the presence of a target. Because of the obvious potential impact of this discovery on the future design of airborne radar, a supporting theoretical study by Dr. Jack Daley at NRL is now being conducted in parallel with this effort to develop and to define sea model parameters which explain the observed data. Results of this study have been very successful in explaining the salient features of the experimental data and consequently provide a better insight to the physical phenomena which control polarization properties of the sea clutter. These studies have also indicated that a rather substantial improvement in signal to clutter ratio of as much as 10 dB may be possible at moderate depression angles where sea clutter is especially troublesome.

The approach used in these studies was based on the changes in the properties of the radar cross section polarization matrix or the "RCS matrix".

The RCS matrix provides a complete description of radar reflectivity of a target. Everyone who has worked with radar targets is familiar with the concept of the "radar cross section area" commonly denoted by the Greek letter σ. This quantity is very useful since it describes in a very simple way the reflectivity of the target to the given radar. Unfortunately σ is not a complete description since in general it is a function of transmitter and receiver polarizations. For instance, if the target is a large flat metal plate at normal incidence, a linearly polarized radar will see a very large σ whereas a circularly polarized radar will see practically nothing since the reflected energy will be cross polarized.

The RCS matrix generalizes the concept of σ and converts the observed relectivity of the target into intrinsic properties of the target independent of the radar. Using RCS matrix parameters, we can by means of mathematical transformations, compute

the target response to any radar whose transmit and receive properties are known.

The method which is used here to present and to describe experimental results presupposes familiarity with RCS matrix, the Poincaré Sphere, polarization space and polarization nulls. For the convenience of readers who are not familiar with these techniques, a brief summary of essential concepts has been included in Appendix A of this report and we do recommend that this material be reviewed before proceeding with the main body of the report.

2.0 DESCRIPTION OF EXPERIMENTAL PROCEDURES

2.1 Site Geometry

The equipment is located on Point Loma at an elevation of 422 feet above mean sea level. Path profiles along three radials are shown in Figure 1. The usable look directions are West ± 20 degrees. To the North the limit is set by the fact that the coastline slopes Westward and only extremely low grazing angles on the sea are possible. To the South there are several large antenna installations close to the site blocking the view of the sea.

Figure 2 is a plot of angle of incidence on the sea surface as a function of range and delay for the actual antenna height of 430 feet above MSL.

To the South and West the maximum incidence angle is about 15 degrees but this is close to the shore. The maximum usable incidence angle is approximately 8 degrees.

2.2 Experimental Equipment

The RCS matrix radar consists of a 10 KW pulse transmitter, a three-channel receiver, and a minicomputer controlled data acquisition and recording system located inside an equipment van.

A ten foot parabolic reflector antenna with a dual polarized square horn feed is used for both transmitting and receiving. The antenna polarizations are 45 degree left and 45 degree right linear. The antenna is mounted on a pedestal with manual pointing capability in azimuth and elevation. A telescope aligned with the electrical axis is used for optical tracking of the antenna pointing.

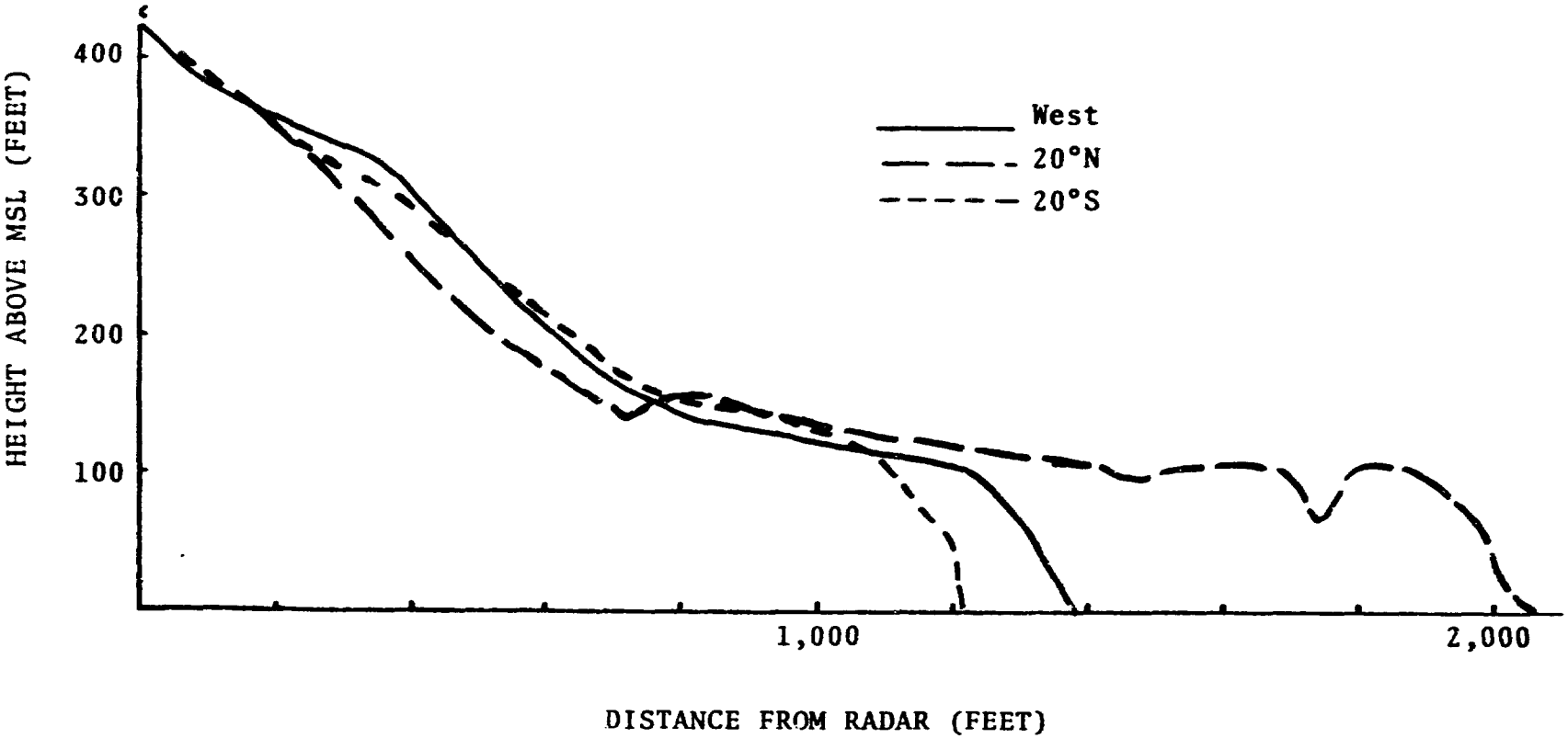

FIGURE 1: Foreground Terrain Profiles - Pt. Loma Site

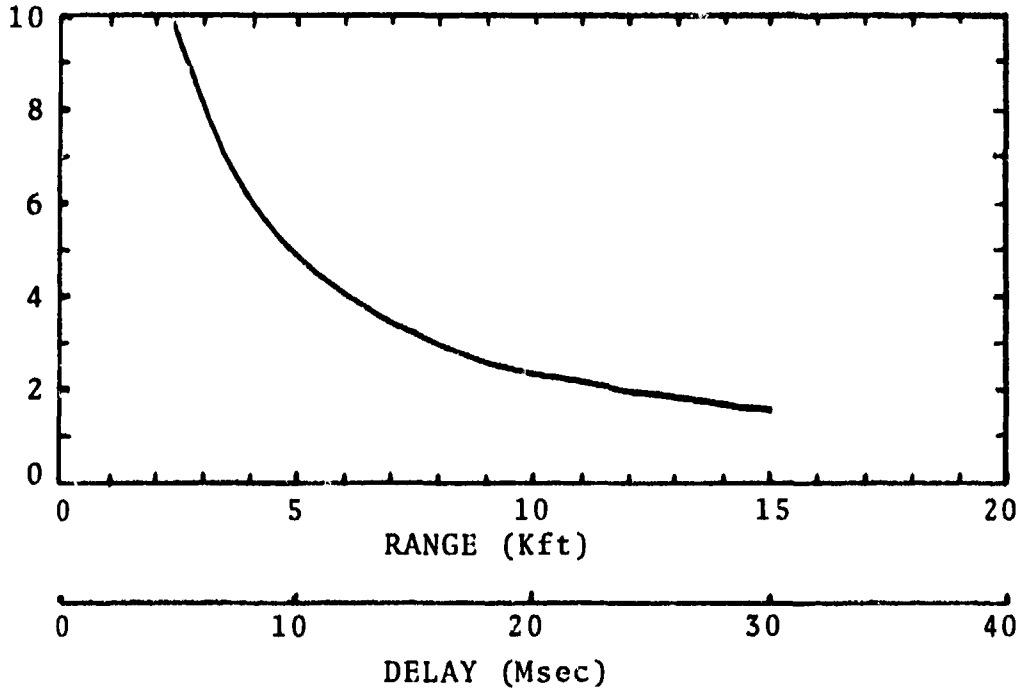

FIGURE 2: Incidence Angle on Sea Surface as Function of Range or Delay. Radar Height = 430'.

The PRF is approximately 3 kHz with a one-half microsecond pulse width. The transmit polarization is switched on every other pulse. The received signal on both polarizations are sampled just prior to switching of the transmit polarization.

The transmitter consists of a CW signal source with approximately 10 mW output. A portion of this signal is coupled off and sent to the receiver for use as a phase and frequency reference. The remainder is pulse modulated. The pulsed signal is amplified to approximately 10 watts in a medium power TWT amplifier. The final stage is a water-cooled solenoid-focused modulating anode traveling wave tube with peak power output of 10 KW and a maximum average power output of 200 watts at 0.25% duty cycle. The operating range of the final stage is 3.1 to 3.5 GHz.

The transmitter output is fed through circulators to the antenna.

The receiver consists of three phase and amplitude matched channels. Each channel consists of a mixer where the input is downconverted to 60 MHz, several stages of IF amplification, coherent quadrature detectors, and two stages of sample-hold circuits. The receiver is operated in a fixed gain mode which provides about 40 dB of dynamic range when some signal averaging is used to reduce the effective noise level. The first local oscillator and 60 MHz coherent detection reference signal are common to the three receiving channels. One of the channels is used for phase and frequency reference and is fed by a coupled off portion of the CW signal. The first sample-hold circuit is a fast attack circuit which uses an externally derived trigger. This sampling time can be delayed a variable amount from the external source thus providing an adjustable range gate. The second sample-hold circuit is a slow decay circuit which is triggered just prior to switching of the polarization. The output of this circuit remains constant

for the period of time required by the A/D conversion in the data acquisition system.

The data acquisition and recording system consists of a multi-channel A/D module, a digital tape recorder, and a NOVA 2 minicomputer. A stored program controls the recording sequence which is initiated by an interrupt pulse that is coincident with the polarization switching signal.

Table I contains a summary of the parameters of the RCS Matrix Radar system as it was configured for these tests. The receiver noise figure is 12 dB and the IF bandwidth is 2 MHz resulting in a receiver noise level of -98 dBm.

2.3 Calibration Procedures

The on-site calibration and equipment check procedures were described in the Second Quarterly Progress Report. Subsequently, it was determined that procedural modifications were required in order to achieve self consistency in the system calibration. For this reason, the basic calibration procedure, with the modifications, will be reviewed in this section.

A knoll in the antenna foreground provides a suitable site for locating standard calibration targets. The geometry of this site is sketched in Figure 3. This site is remarkably free of multipath. A field probe when illuminated by the radar antenna essentially reproduces the antenna patterns with no evidence of ground reflections. The background is rather high but is sufficiently constant to allow its subtraction from the calibration data.

The procedure utilizes measurements on three known targets, the background, and no signal conditions, with a fourth known target (a dipole) used for ambiguity resolution.

TABLE I

RCS MATRIX RADAR PARAMETERS

$$P_R = (P_T G_T G_R \lambda^2 \sigma)/(64\pi^3 R^4 L_T L_R)$$

where

P_R = Signal power at input to receiver

P_T = Power at output of transmitter = 10 KW = +70 DBM

G_T = Transmitter antenna gain = 36.5 dB

G_R = Receiver antenna gain = 36.5 dB

λ = Radio wavelength = .09m

R = Radar range

L_T = Losses between transmitter and antenna = 10 dB

L_R = Losses between antenna and receiver = 5 dB

σ = Clutter backscatter cross section = $\sigma_o A$

σ_o = Clutter cross section per unit area of sea surface

A = Illuminated area on the sea surface

$A = (\alpha R \beta)(C\tau \sec\psi/2)$

β = 3 dB azimuth beamwidth in radians = .037

α = A weighting factor $1/\sqrt{2}$

C = Velocity of light

τ = RF pulse width = 0.5 μs

and

ψ = Incidence angle in the sea surface.

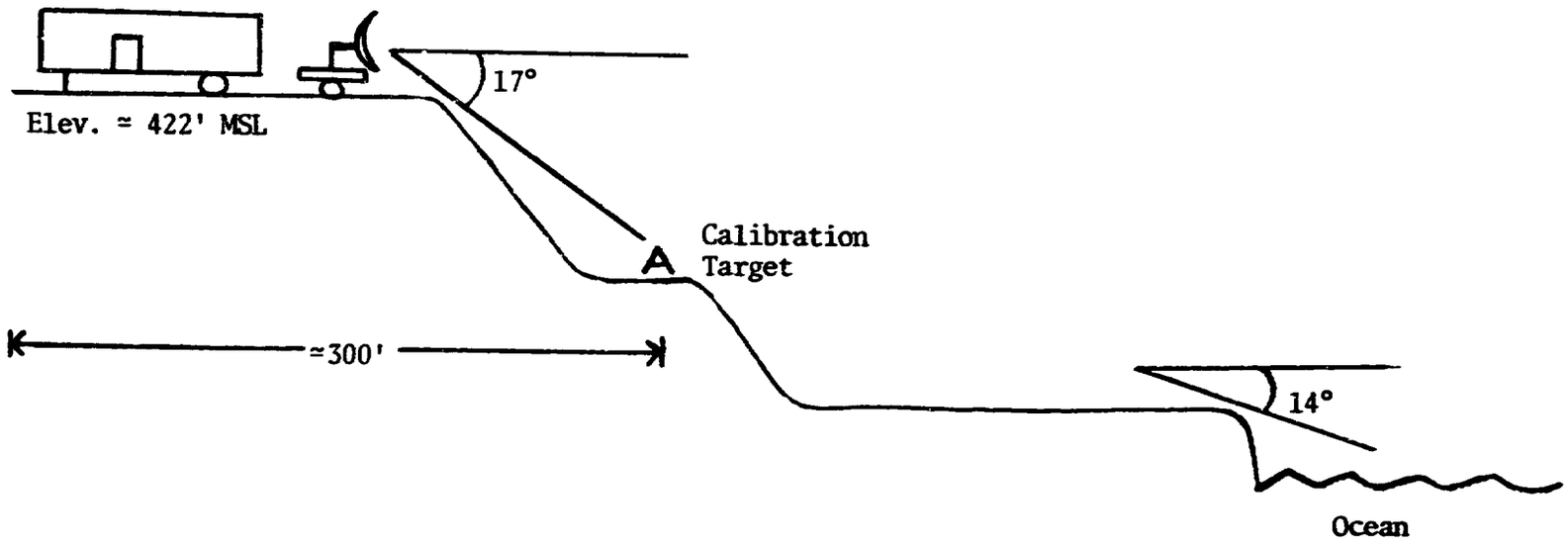

FIGURE 3
GENERAL SITE TOPOGRAPHY

The three known targets are a reference flat plate (a sphere may also be used), a dihedral with its axis in the vertical plane, and a dihedral with its axis rolled out of the vertical plane. The data from these targets together with the background and no signal condition data is adequate to completely determine the system parameters. This is done in the following fashion:

For a linear system the measured RCS matrix (σ') when the true RCS matrix is σ is given by

$$\sigma' = D\sigma C + \Gamma \qquad (1)$$

where Γ = receiver output matrix when there is no target
D = transmitter coupling matrix
and C = receiver coupling matrix.

The matrix Γ represents the combined effects of D.C. offsets in the coherent detectors, transmit to receiver leakage, etc. The matrix D describes the transmitter coupling, differential gain, etc. That is, if the nominal transmitted polarization is i then the field component with polarization j is D_{ij}. Similarly, the C matrix describes the response of the receiving system to the field scattered by the target. Thus, C_{ij} is the response in receiver channel j when the scattered field has polarization i.

The offset matrix Γ is determined by recording with no targets in the range gate. The transmitter and receiver coupling matrices are determined by recording data from a set of standard targets whose RCS matrices are known. Although in principle two properly chosen targets should provide enough information to uniquely define the unknown parameters we have been unable to find a set with fewer than three targets which leads to an unambiguous solution.

The three standard targets which we utilize are a flat plate, a dihedral with its axis vertical, and a dihedral with its axis rolled at an arbitrary angle θ about an axis parallel to the line of sight.

The flat circular plate provides an absolute cross section reference and is used here also as a phase reference. When the orthogonal antenna polarizations are horizontal (H) and vertical (V) the normalized flat plate RCS matrix is

$$\sigma^F = \begin{pmatrix} 1 & 0 \\ 0 & 1 \end{pmatrix} \tag{2}$$

Using the flat plate as a reference the RCS matrix of the vertical dihedral ($\theta = 0$) is

$$\sigma^O = A_o \begin{pmatrix} -1 & 0 \\ 0 & 1 \end{pmatrix} \tag{3}$$

and the dihedral rolled through an angle θ is

$$\sigma^\theta = A_\theta \begin{pmatrix} -\cos 2\theta & -\sin 2\theta \\ -\sin 2\theta & -\cos 2\theta \end{pmatrix} \tag{4}$$

The constants A_o and A_θ are complex numbers. If the dihedrals are properly oriented their amplitudes are known and equal. Their phases, however, are usually uncertain because of the practical difficulties of positioning the phase center of the dihedral coincident with that of the flat plate. In our procedures we allow both the amplitudes and phases to the unknown.

From Equations 2 through 4 it follows that

$$|A_o|^2 = -|\sigma^o|/|\sigma^F| \tag{5}$$

and

$$A_\theta|^2 = -|\sigma^\theta|/|\sigma^F|. \tag{6}$$

Furthermore, these same relationships apply if we replace σ by $\sigma-\Gamma$ so that the unknown constants A_o and A_θ may be determined (with a phase ambiguity of 180 degrees) from the determinants of the measured RCS matrices. In the following discussion we will assume that this has been done and all of the matrices have been normalized. We further assume that the offset matrix, Γ, has been found and subtracted from the measured RCS matrices.

When Equations 2 through 4 are inserted into Equation 1 then we find 12 complex equations (not all independent) in 7 complex unknowns. The complex unknowns are the elements of the C and D matrices with the recognition that one of these elements may be arbitrarily chosen since only products are of significance. One form of the 12 equations is Equation 7 through 18 with the ε's set equal to zero. If there were no noise or measurement errors it would be possible to solve these equations for the unknowns. Since there are measurement errors and noise, however, a best fit solution is found. That is, the unknown matrix coefficients and the angle θ are determined by minimizing the quantity E where

$$E = \sum_{1}^{12} |\varepsilon_i|^2$$

and the ε's are given by Equations 7 through 18. Since the minimization equations are nonlinear we use an iterative solution algorithm.

$$\varepsilon_1 = \sigma_{11}^{H} - C_{21}D_{12} \tag{7}$$

$$\varepsilon_2 = \sigma_{12}^{H} - C_{22}D_{12} \tag{8}$$

$$\varepsilon_3 = \sigma_{21}^{H} - C_{21}D_{22} \tag{9}$$

$$\varepsilon_4 = \sigma_{22}^{H} - C_{22}D_{22} \tag{10}$$

$$\varepsilon_5 = \sigma_{11}^{V} - C_{11}D_{11} \tag{11}$$

$$\varepsilon_6 = \sigma_{12}^{V} - C_{12}D_{11} \tag{12}$$

$$\varepsilon_7 = \sigma_{21}^{V} - C_{11}D_{21} \tag{13}$$

$$\varepsilon_8 = \sigma_{22}^{V} - C_{12}D_{21} \tag{14}$$

$$\varepsilon_9 = \sigma_{11}^{\theta} + D_{11}R_{11} + D_{12}R_{21} \tag{15}$$

$$\varepsilon_{10} = \sigma_{12}^{\theta} + D_{11}R_{12} + D_{12}R_{22} \tag{16}$$

$$\varepsilon_{11} = \sigma_{21}^{\theta} + D_{21}R_{11} + D_{22}R_{21} \tag{17}$$

$$\varepsilon_{12} = \sigma_{22}^{\theta} + D_{21}R_{12} + D_{22}R_{22} \tag{18}$$

where $\sigma^H = (\sigma^F + \sigma^O)/2$

$\sigma^V = (\sigma^F - \sigma^O)/2$

$R_{11} = C_{11}C + D_{21}S$

$R_{12} = C_{12}C + C_{22}S$

$R_{21} = C_{11}S - C_{21}C$

$R_{22} = C_{12}S - C_{22}C$

$C = \cos(2\theta)$

and $S = \sin(2\theta)$.

A figure of merit for the goodness of the data is the ratio of E to the total power in the three target matrices.

Equations 3 and 4 are for ideal dihedrals. The RCS matrix of a real dihedral will differ slightly from these forms due to the presence of a non-specular flat plate component. Figure 4 shows the geometry of this component.

The specular component cross-section of the dihedral is given by [1]

$$\sigma_s \approx 4\pi \ (A/\lambda)^2$$

where A = area of one side

and λ = radar wavelength.

The non-specular component cross-section is oscillatory with frequency and size and is not well defined. If the two sides behaved independently formulae given by Ross[2] could be used and would predict a polarization dependence. The fact that the two sides are joined, however, must substantially alter the contributions of diffraction at the edges. The magnitude of the components can be estimated from physical optics theory and is found to be

$$\sigma_{ns} = 2\sigma_s \left[\frac{\sin(ka/\sqrt{2})}{ka/\sqrt{2}}\right]^2$$

where $k = 2\pi/\lambda$

and a = length of one side.

---

(1) Ruck, G. T., Barrick, D. E., Stuart, W. D., and Krichbaum, C. D.; Radar Cross Section Handbook, Plenum Press, New York (1970).

(2) Ross, R. A., "Radar Cross Section of Rectangular Flat Plates as a Function of Aspect Angle", IEEE Transactions on Antennas and Propagation, Vol. AP-1r, No. 3, pp 329-335 (1966).

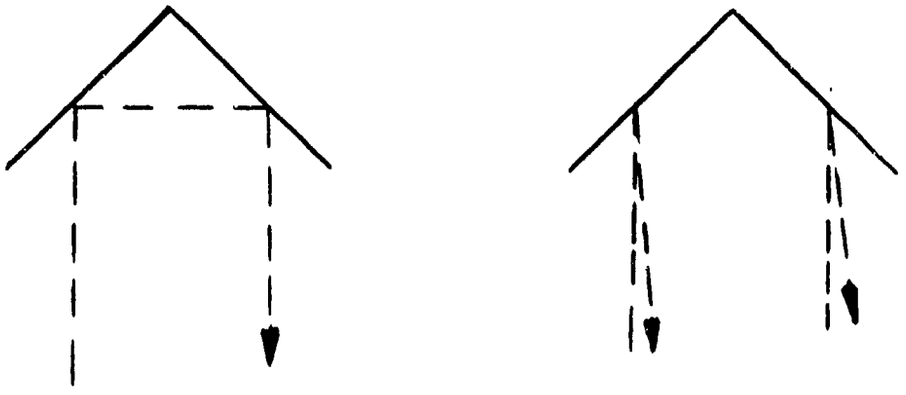

Figure 4

Geometry of specular and non-specular Components of Reflection from a Dihedral.

For the dihedral used in these calibrations these results predict a non-specular return which is of the order of 25 dB smaller than the specular return. When this was not taken into account when applying the theory, the residual errors after performing a least squares fit were found to always be of the order of 25-30 dB below the total power in the three target matrix. If the non-specular component is assumed to be independent of polarization then the total cross section matrix of the dihedral will consist of the sum of two terms of the form of (2) and (4). The difference between measurements made a 0 and 0+90° will then cancel out the non-specular term and the specular terms will add. When this was done the residual errors were reduced 10 dB resulting in considerable enhanced confidence in the calibrations.

The calibration procedure utilized then should consist of measuring a flat plate, the background, and dihedrals at roll angles of 0, 45, 90, and 135 degrees. The difference between the roll 0 and roll 90 dihedral data is designated as roll 0 and the difference between the roll 45 and roll 135 dihedral data is designated as roll 45. This data is then used in the procedure described in the preceding paragraphs.

This modification of the procedure was developed after the last data on this contract was taken but will be used in further tests.

3.0 PRELIMINARY EXPERIMENTAL RESULTS

During the last stages of equipment check out at the NOSC site there were several opportunities to gather some preliminary data on sea clutter and on targets of opportunity. The data presented here consists of four samples of clutter taken at depression angles 2.9°, 3.3°, 4.1° and 6.1° respectively and three targets of opportunity: a sailboat, a launch with big wake and a sportfishing boat. The sea conditions were fairly calm and the return from the targets was in general well above the clutter level, especially since the targets were further out in range near grazing incidence where the clutter level tended to be low.

Approximately .6 seconds of representative data were selected for the purpose of illustrating the RCS matrix properties of the above mentioned clutter samples and targets of opportunity.

To facilitate the discussion, each RCS matrix data sample utilizes a similar four page format which consists of one page of amplitude information and three pages of polarization information. This is described below.

3.1 Data Format

Experimental data discussed in Sections 3.2 and 3.3 is presented with the aid of two types of supplementary formats: amplitude and null polarizations. These two formats will now be explained in detail.

A typical amplitude format is illustrated by Figure 5a. The format displays amplitude of RCS matrix elements as a function of data sample number for about 600 consecutive data points (300 in each of the two columns). Because of the high degree of correlation in the amplitude values of adjacent data points only every fifth data sample is printed out and every 25th is

identified by a number on the left margin. The data rate was approximately 1,000 RCS matrix samples per second so that as a convenient approximation the data number represents time in milliseconds.

The horizontal scale at the top of each record represents relative amplitude. Vertical rows of dotted lines represent amplitude steps of 10 dB. There are ten horizontal character spaces between the dotted lines so that each horizontal space represents a step of one dB.

Although, because of engineering considerations, the RCS matrix data was collected using $\pm 45°$ linear polarizations, the data shown here is the data which has been corrected by system calibration and which has been polarization rotated to show what would have been recorded with a radar using horizontal and vertical polarizations.

The symbols are as follows:

$$H = |\sigma_{HH}|$$
$$V = |\sigma_{VV}|$$
$$X = |\sigma_{HV}| = |\sigma_{VH}|$$
$$S = [|\sigma_{HH}|^2 + |\sigma_{VV}|^2 + 2|\sigma_{HV}|^2]^{1/2}$$

where $|\sigma_{ij}|$ represents radar cross section observed with the i^{th} polarization transmitted and j^{th} polarization received. Here subscripts H and V denote horizontal and vertical polarizations respectively.

In data samples when the total target reflectivity, "S", is not printed out, S occupies the same amplitude cell as the strongest component shown. In general, when two or more letters occupy the same amplitude space only one will be printed in the following order of precedence: X, V, H, S and · (dot).

The second type of data format used here is exemplified by Figure 5b and displays in rectilinear coordinates the latitude and longitude of the co and cross pol nulls on the Poincare Sphere (See the Appendix for discussion of co and cross pol nulls and Poincaré Sphere). The four plots on the left side of the page represent co pol nulls and those on the right show the cross pol nulls. Each plot shows 50 consecutive data points identified by the numbers below each plot. These data point numbers represent the same points on the corresponding amplitude data points. Thus each of the same 600 data points shown on the amplitude charts are re-examined in the polarization space on the Poincaré Sphere. For convenience the 50 points are consecutively labeled "A, B,B, C,C, D,D,.....X,X, Y,Y, Z." (There is only one A and Z). It will be recalled that only 10 of these 50 points in each plot are printed out on the amplitude plots. These ten points are:

1 - second C	6 - first P
2 - first F	7 - second R
3 - second H	8 - first U
4 - first K	9 - second W
5 - second M	10 - Z

Each of the 72 horizontal spaces in the plots represents a five degree step in longitude and each of the 18 vertical spaces in the plot represents a five degree step in latitude. In cases where two or more letters occupy the same horizontal and vertical space only the highest ranking letter is printed.

To summarize, the data associated with each clutter and target sample discussed here is illustrated by a set of four page figures labeled a, b, c, and d. The first page is the amplitude data showing 600 consecutive data points and representing approximately 600 milliseconds of data. The other three pages detail the polarization properties of each of the 600 points (200 per page) by the use of co and cross pol null coordinates plots on the Poincare Sphere with 50 consecutive data points per plot.

3.2 Target Data

As stated earlier, observations were made on three different targets of opportunity: a sailboat, a launch and a sportfishing boat. Figure 5a, 6a, and 7a show samples of the amplitude data. (See Section 3.1 for format explanation). The amount of structure appears to be directly related to the target complexity. The sailboat exhibits very little fluctuation in total target reflectivity(s), although the $|\sigma_{VV}|$ tends to fade more than $|\sigma_{HH}|$. The cross pol component $|\sigma_{HV}|$ is in general much weaker. Both the launch and the sportfishing boat exhibit quasi periodic fading with the sportfishing boat showing more structure than the launch. The period of fading appears to be on the order of 75 milliseconds which would seem to suggest that it is generated by the relative motion of scatter centers moving in opposite sense relative to the receiver with the velocity of about two feet per second which probably is a reasonable value for a 60 to 80 foot boat tossed up and down by wave action.

Polarization plots of co and cross pol nulls shown in Figures 5b,c,d, 6b,c,d, and 7b,c,d are interesting. In the case of the sailboat the copol nulls appear to cluster in the polar region, a condition reminiscent of a near specular reflection from a flat surface. A notable exception to this occurs in point sequence of 450-650 which when examined in the amplitude domain shows a significant fade of the $|\sigma_{VV}|$ component followed by a fade of $|\sigma_{HH}|$ component.

The cross pol plots exhibit well defined clustering in the equatorial region throughout the entire sequence except that during the 400-650 fade cycle which shows a distinct progression of the cluster eastward (to the right).

The polarization characteristics of the launch are distinctly different from the sailboat. There is much less

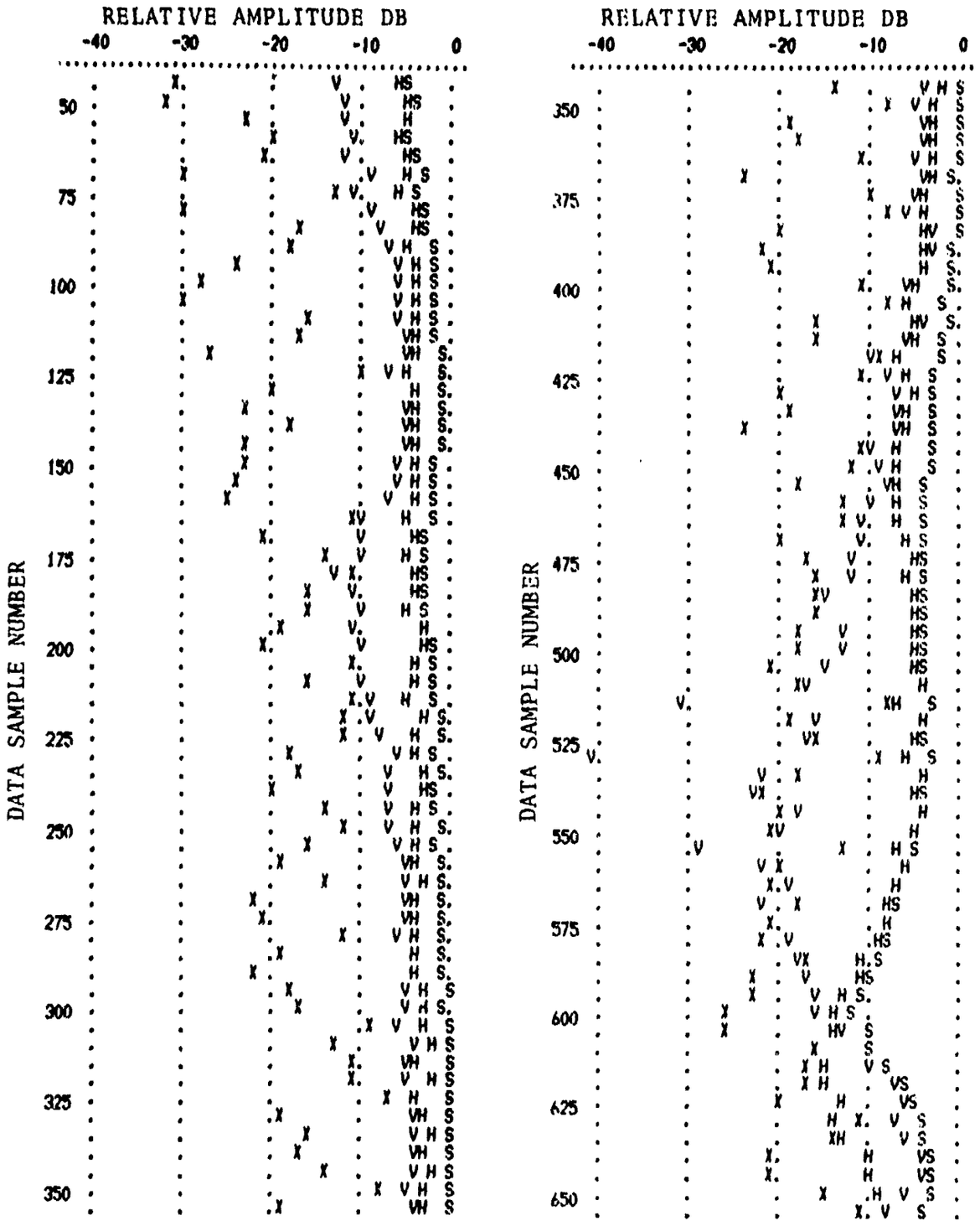

FIGURE 5a - Sailboat Signal Amplitude; Angle of Elevation = 1.5

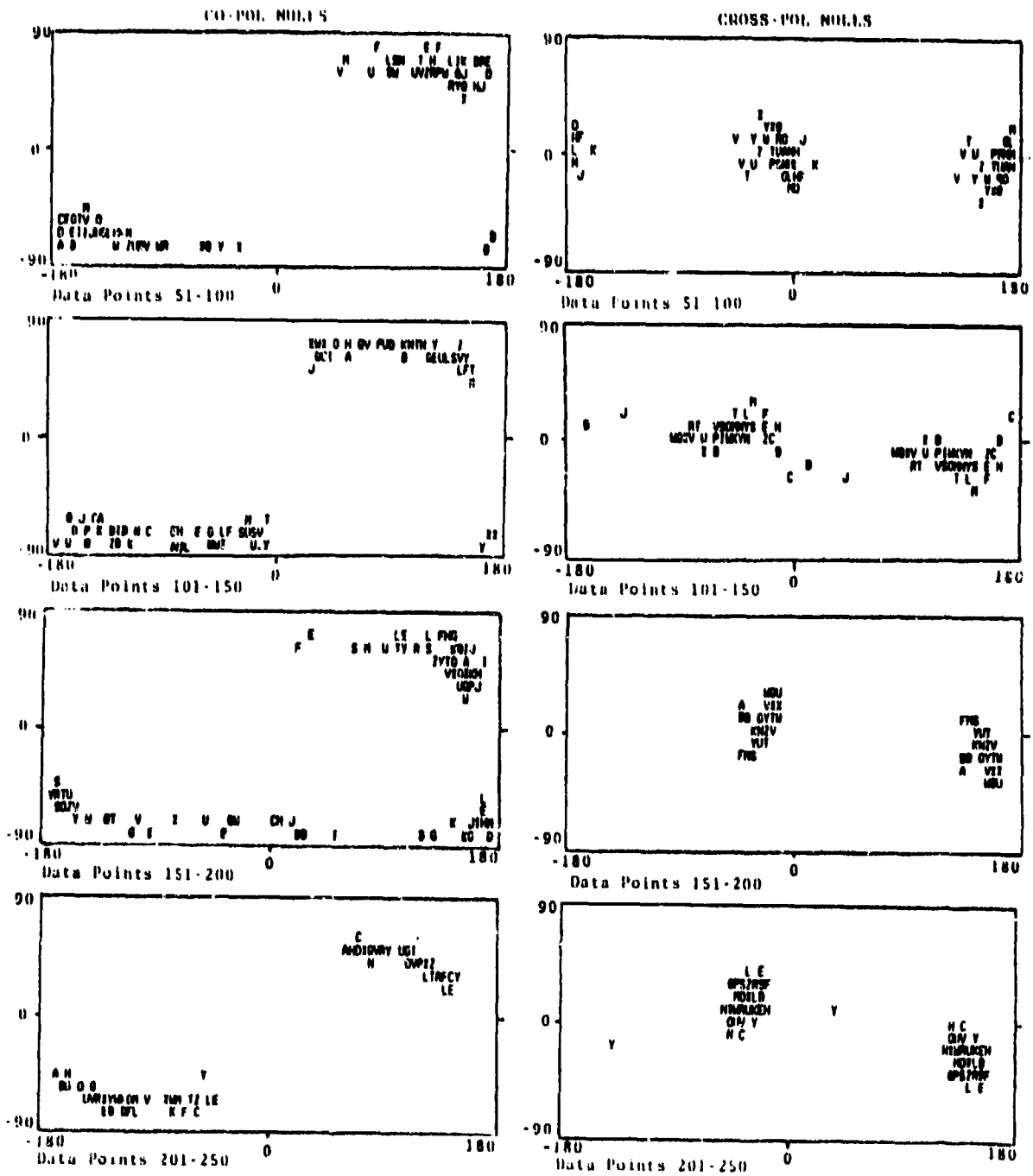

FIGURE 5b - Sailboat Polarization Nulls
Data Points 51-250

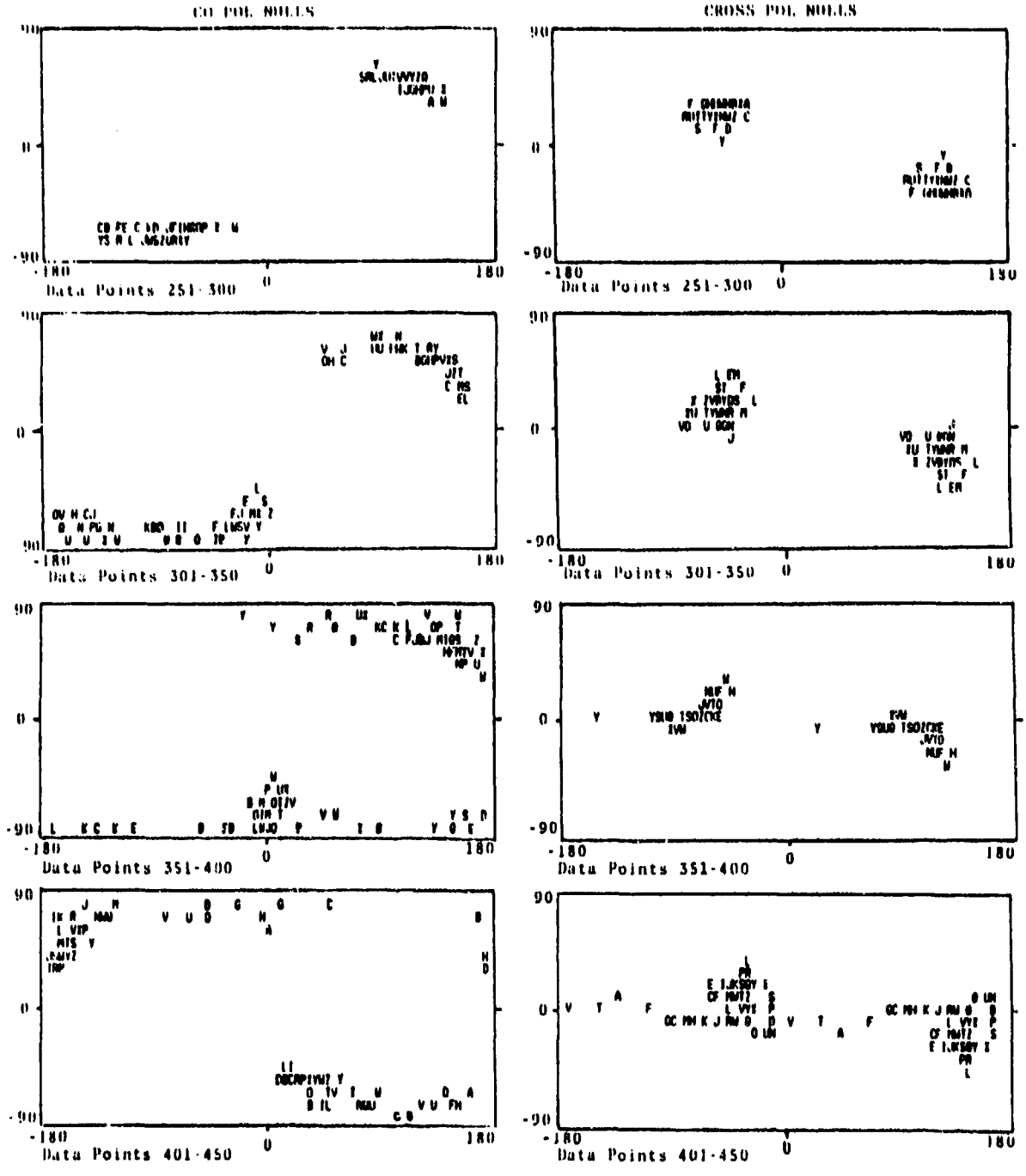

FIGURE 5c - Sailboat Polarization Nulls
Data Points 251-450

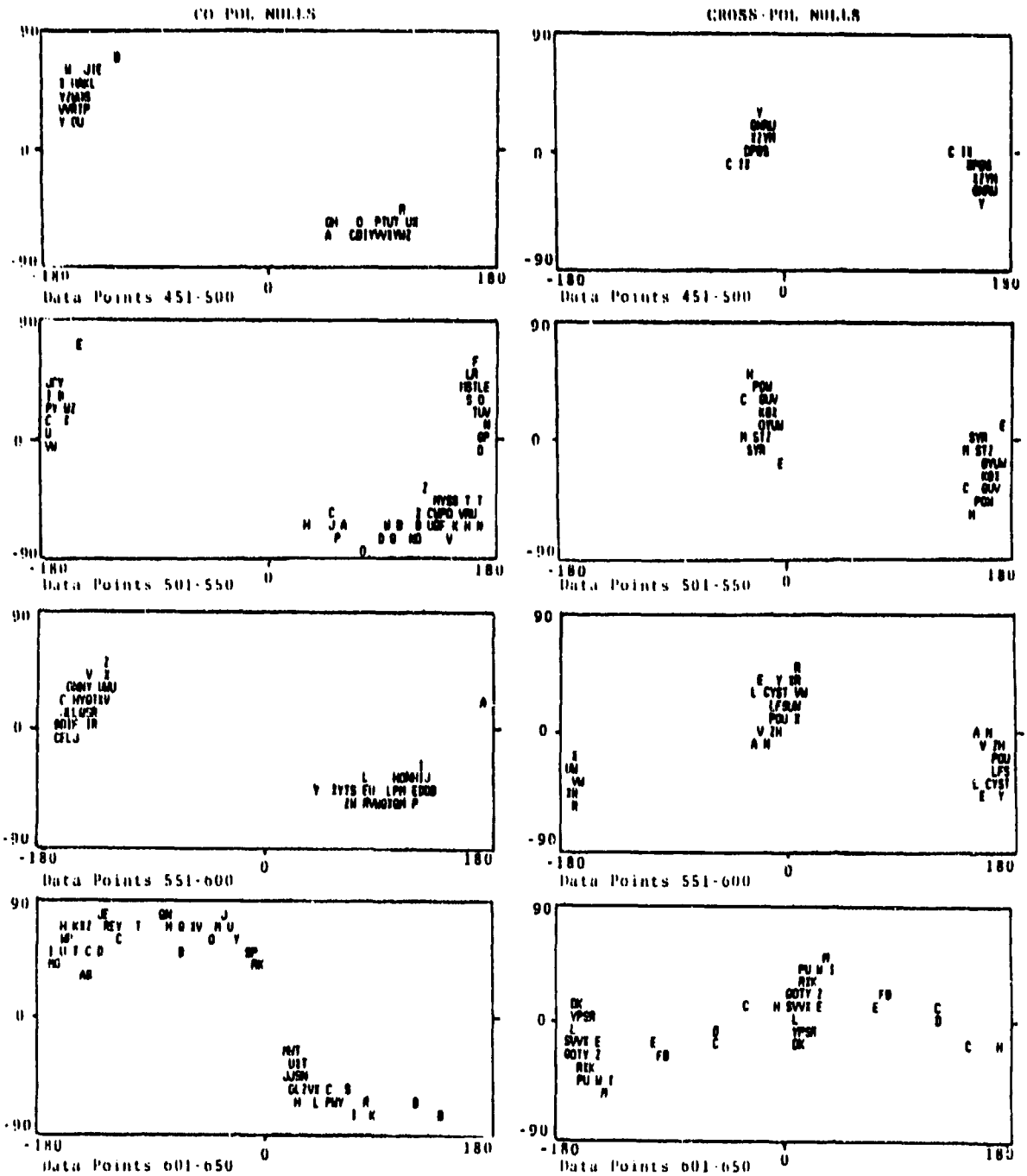

FIGURE 5d - Sailboat Polarization Nulls
Data Points 451-650

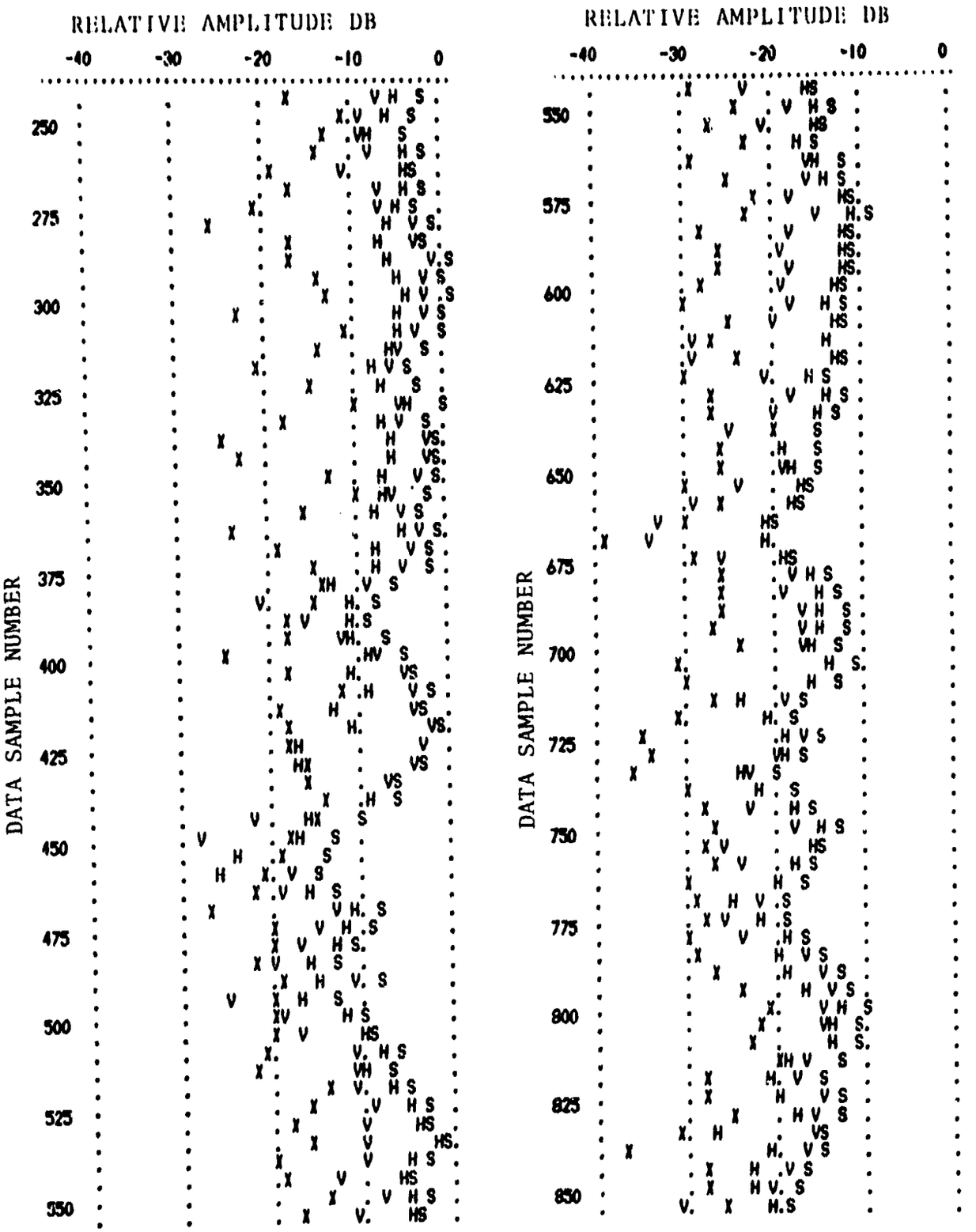

FIGURE 6a - Launch Signal Amplitude; Angle of Elevation = 1.5

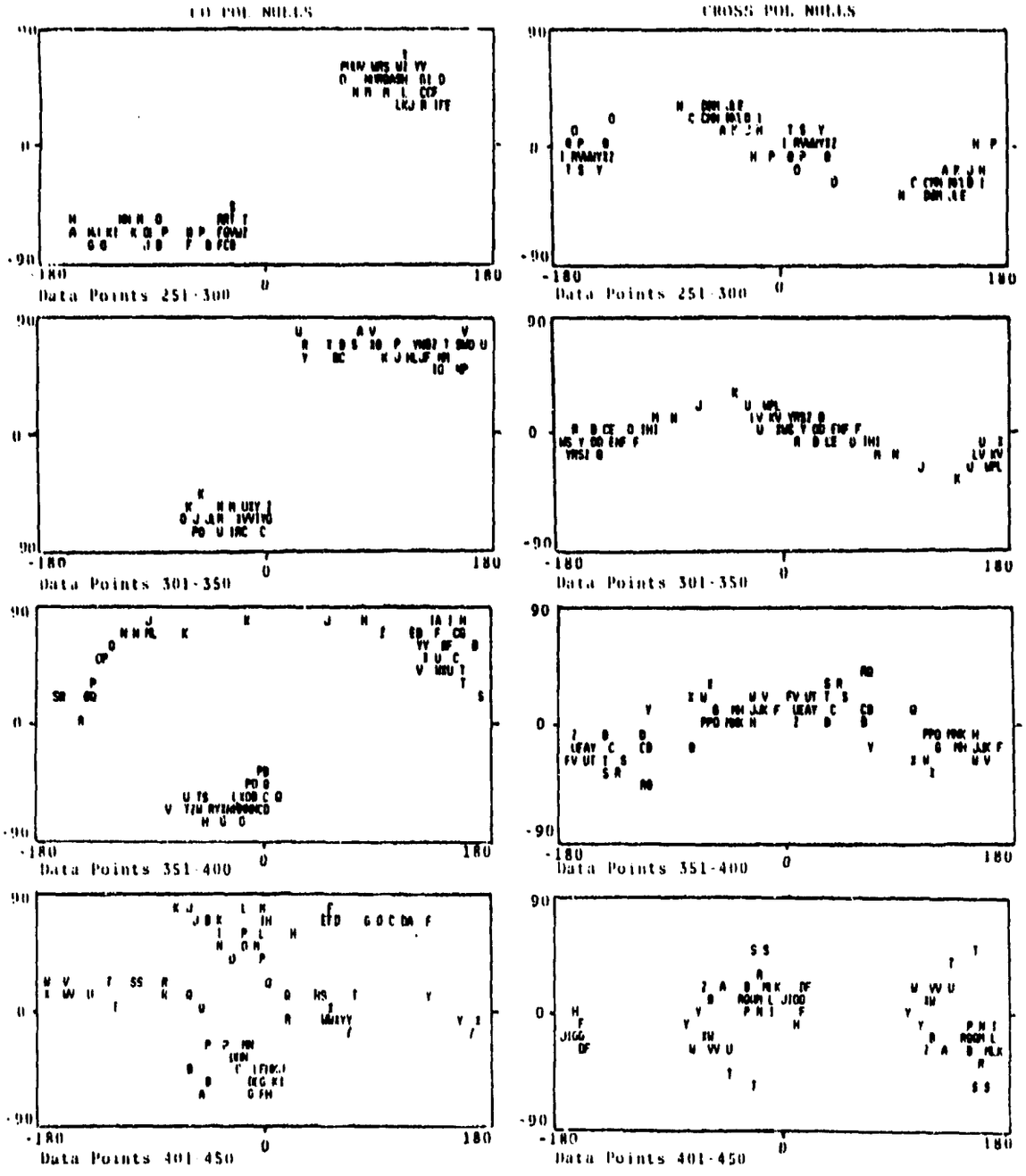

FIGURE 6b - Launch Polarization Nulls
Data Points 251-450

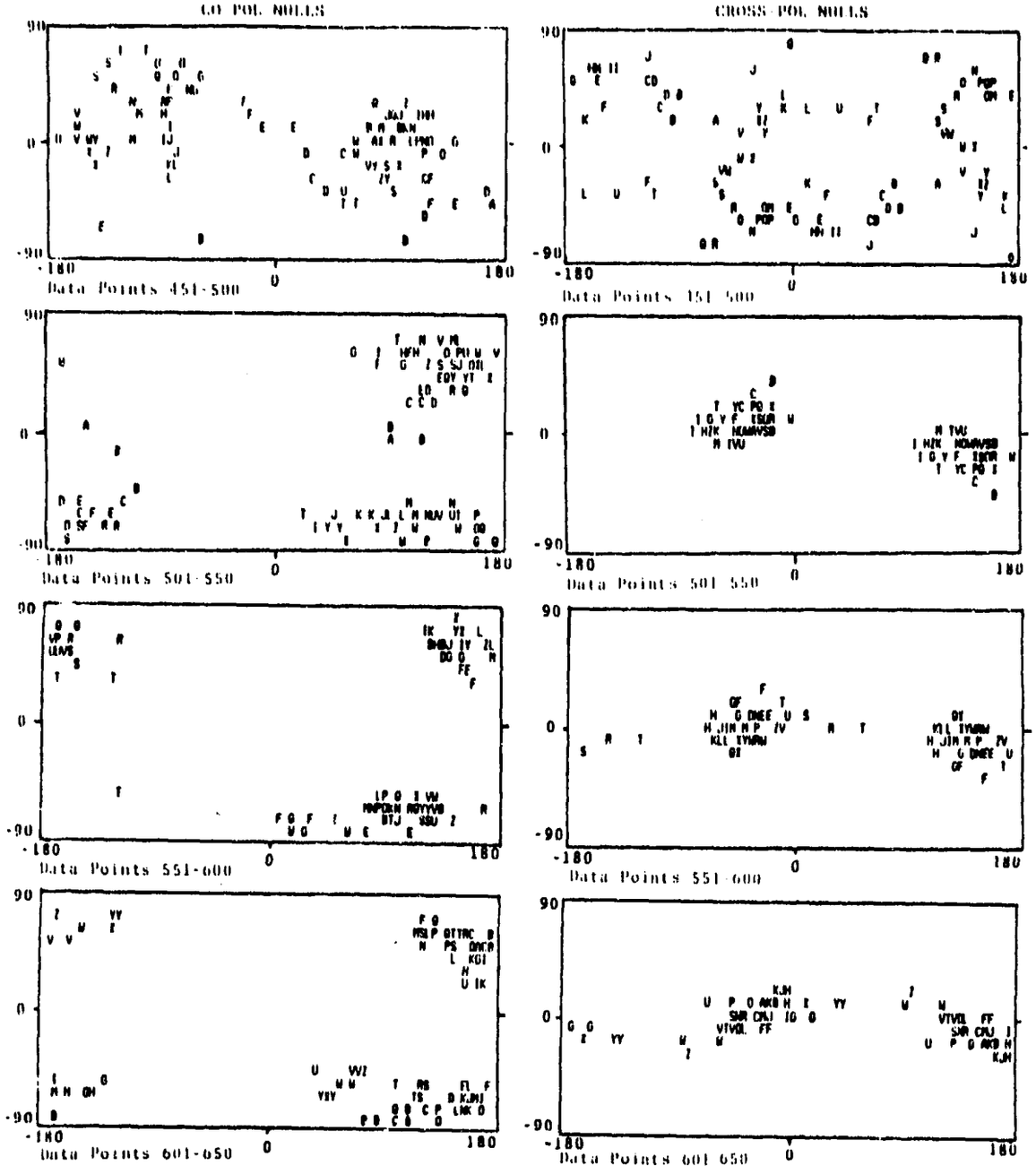

FIGURE 6c - Launch Polarization Nulls
Data Points 451-650

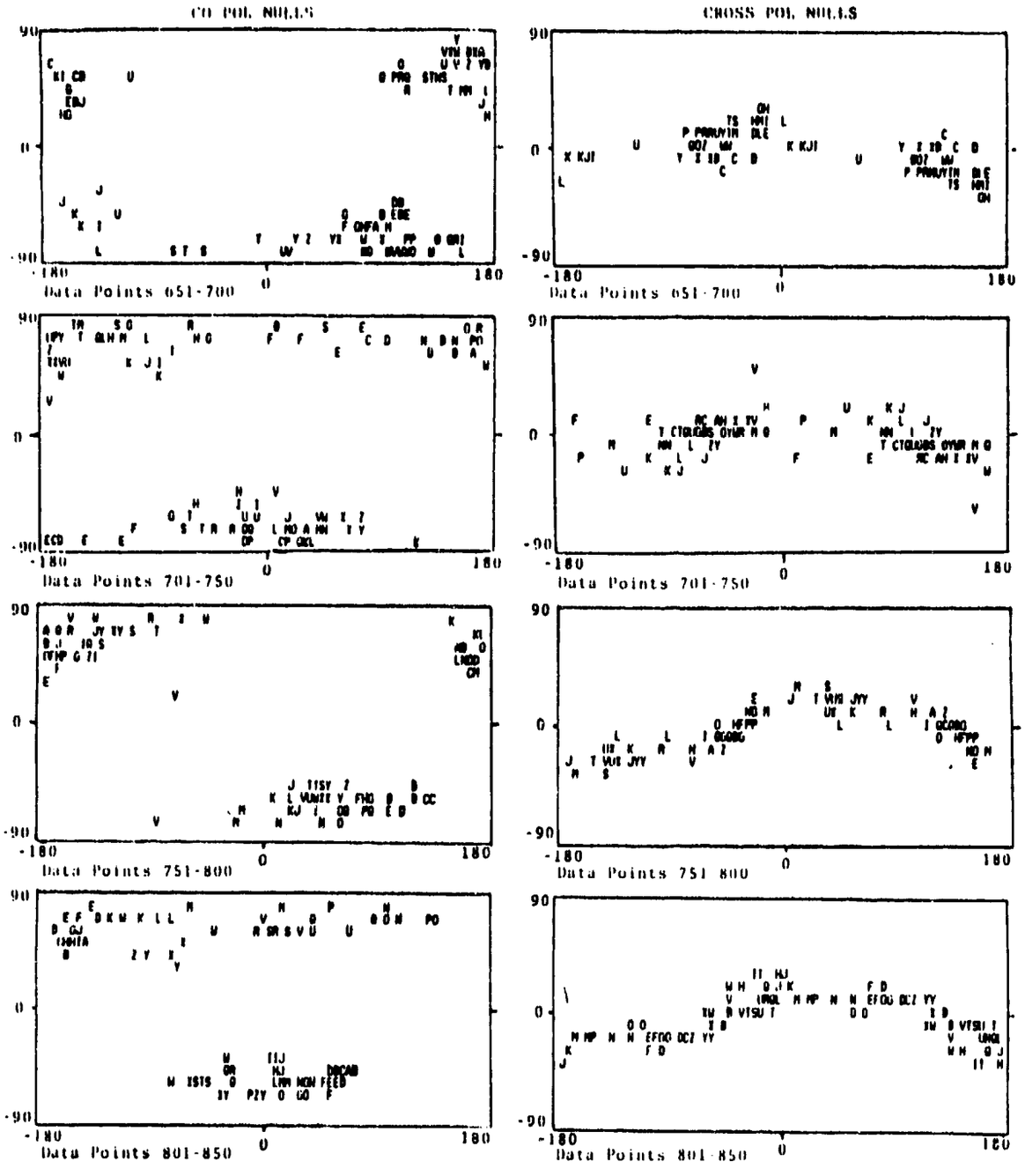

FIGURE 6d - Launch Polarization Nulls
Data Points 651-850

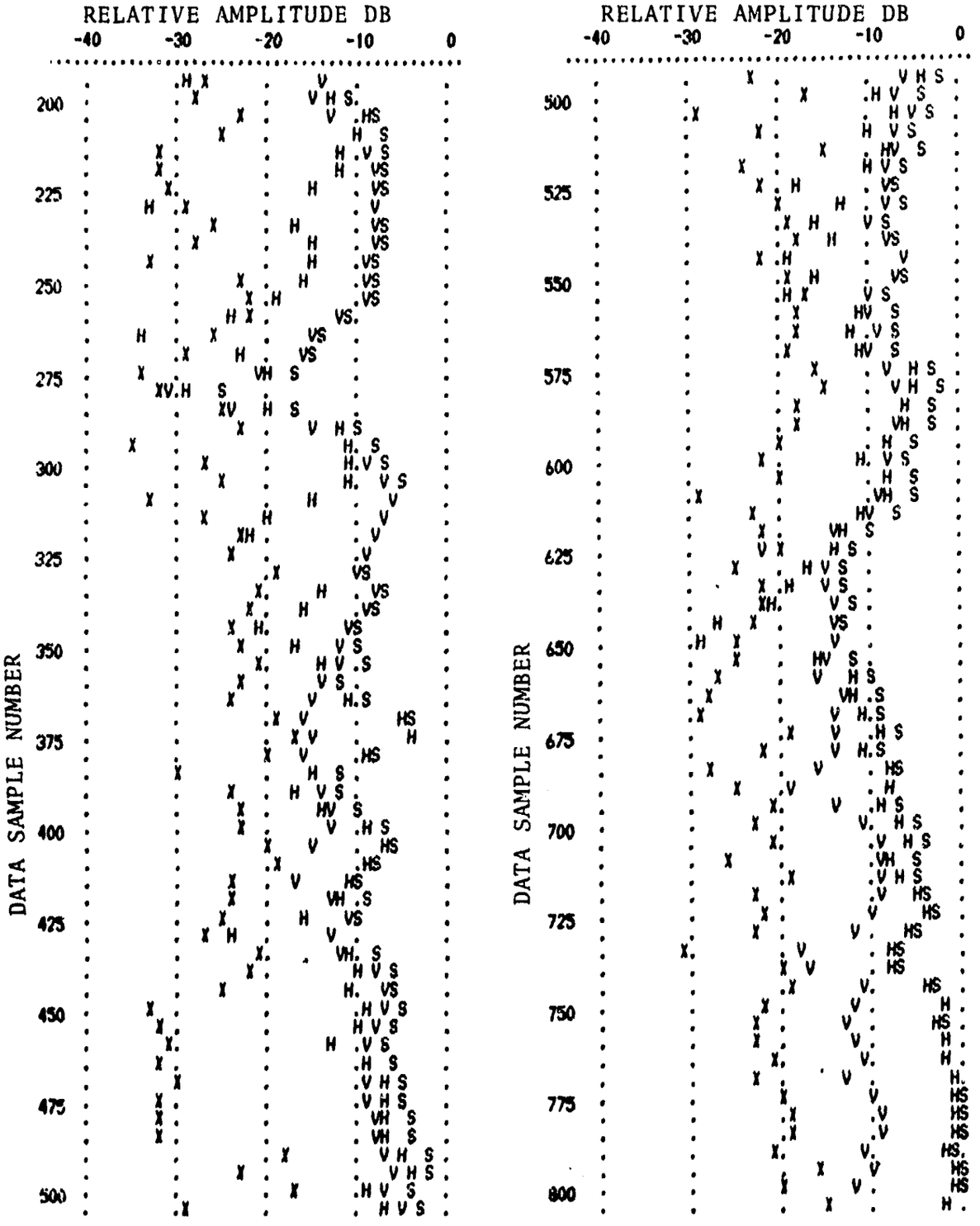

FIGURE 7a - Sport Fishing Boat Signal Amplitude;
Angle of Elevation = 1.5

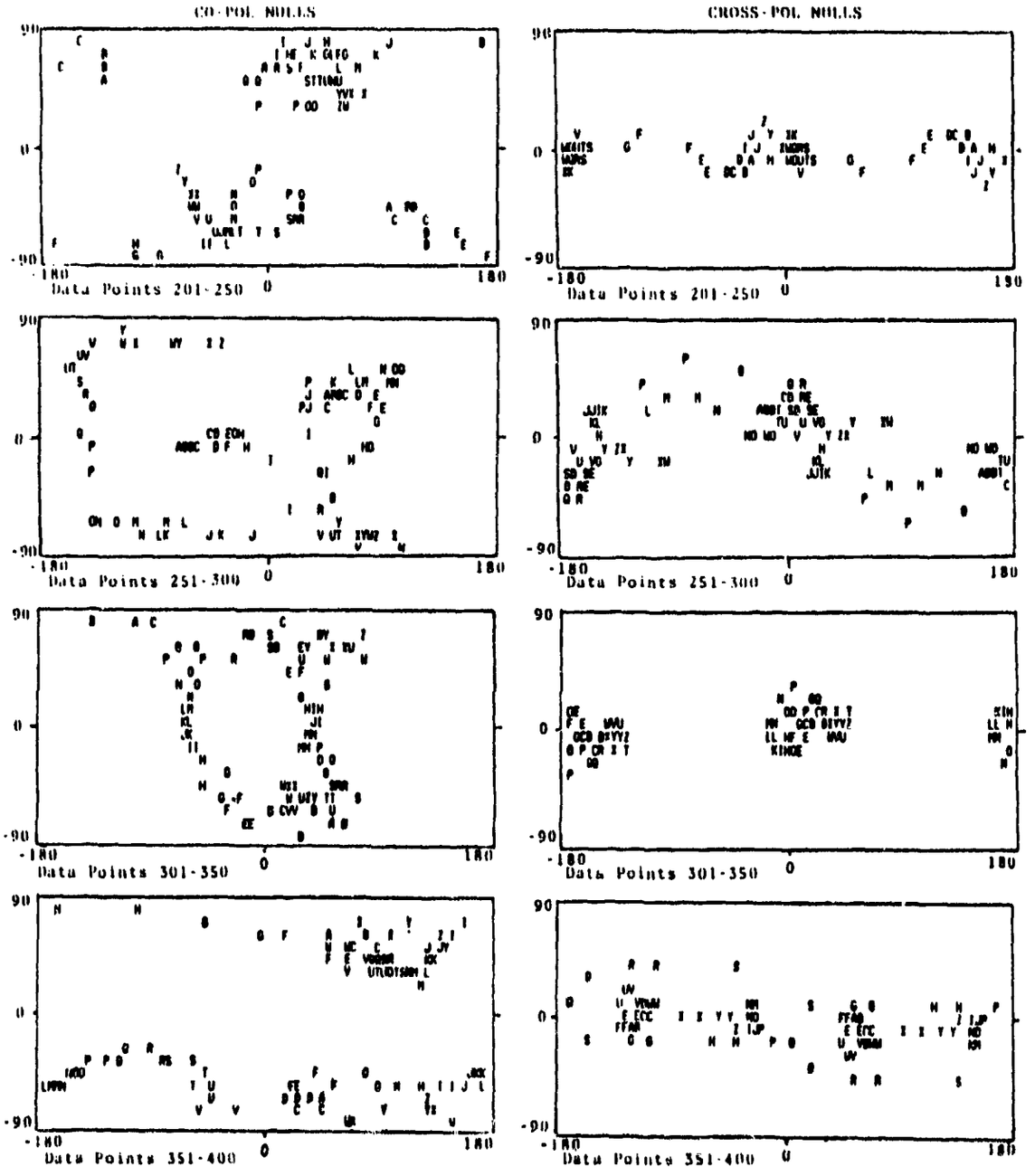

FIGURE 7b - Sportfishing Boat Polarization Nulls
Data Points 201-400

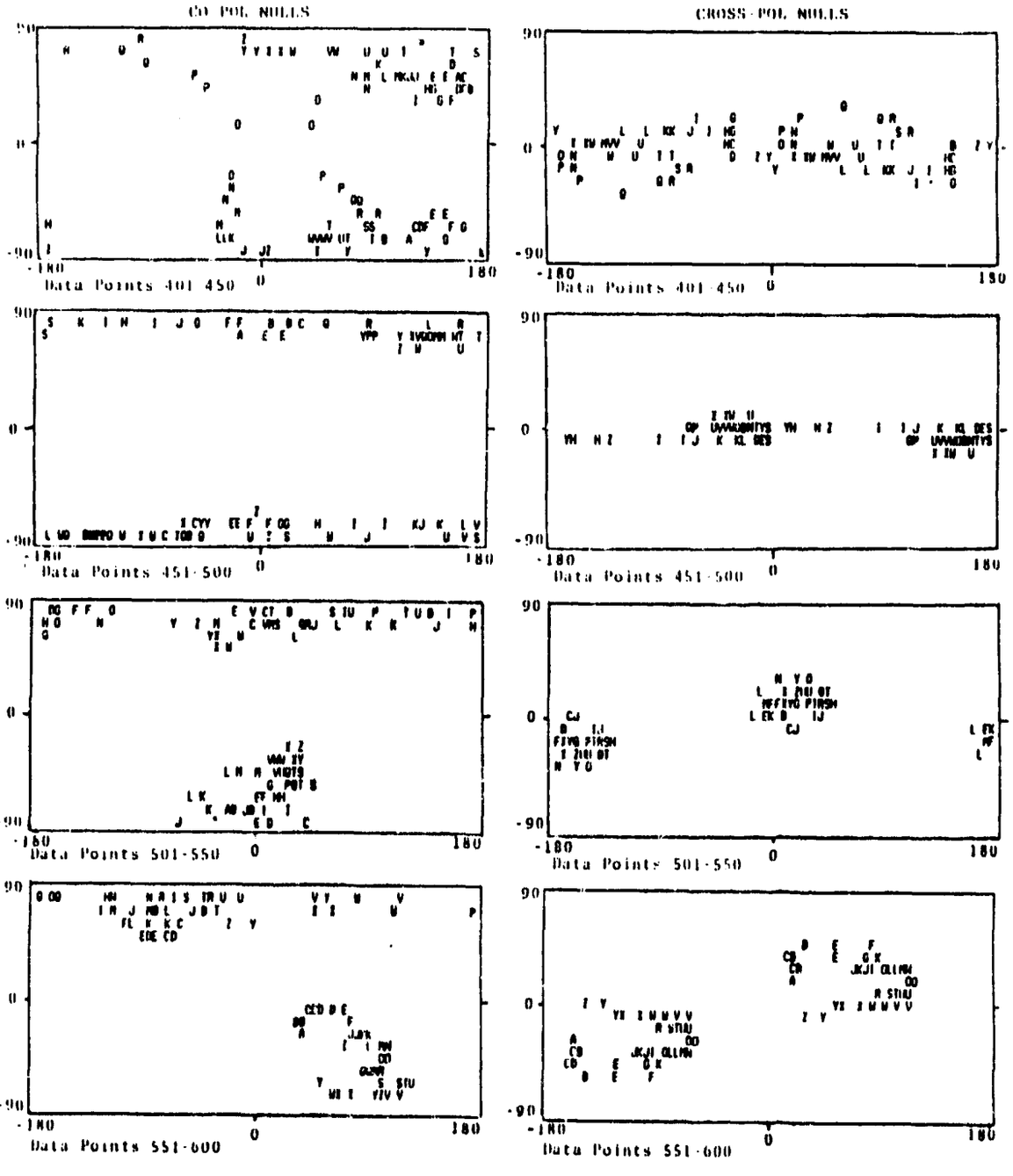

FIGURE 7c - Sportfishing Boat Polarization Nulls
Data Points 401-600

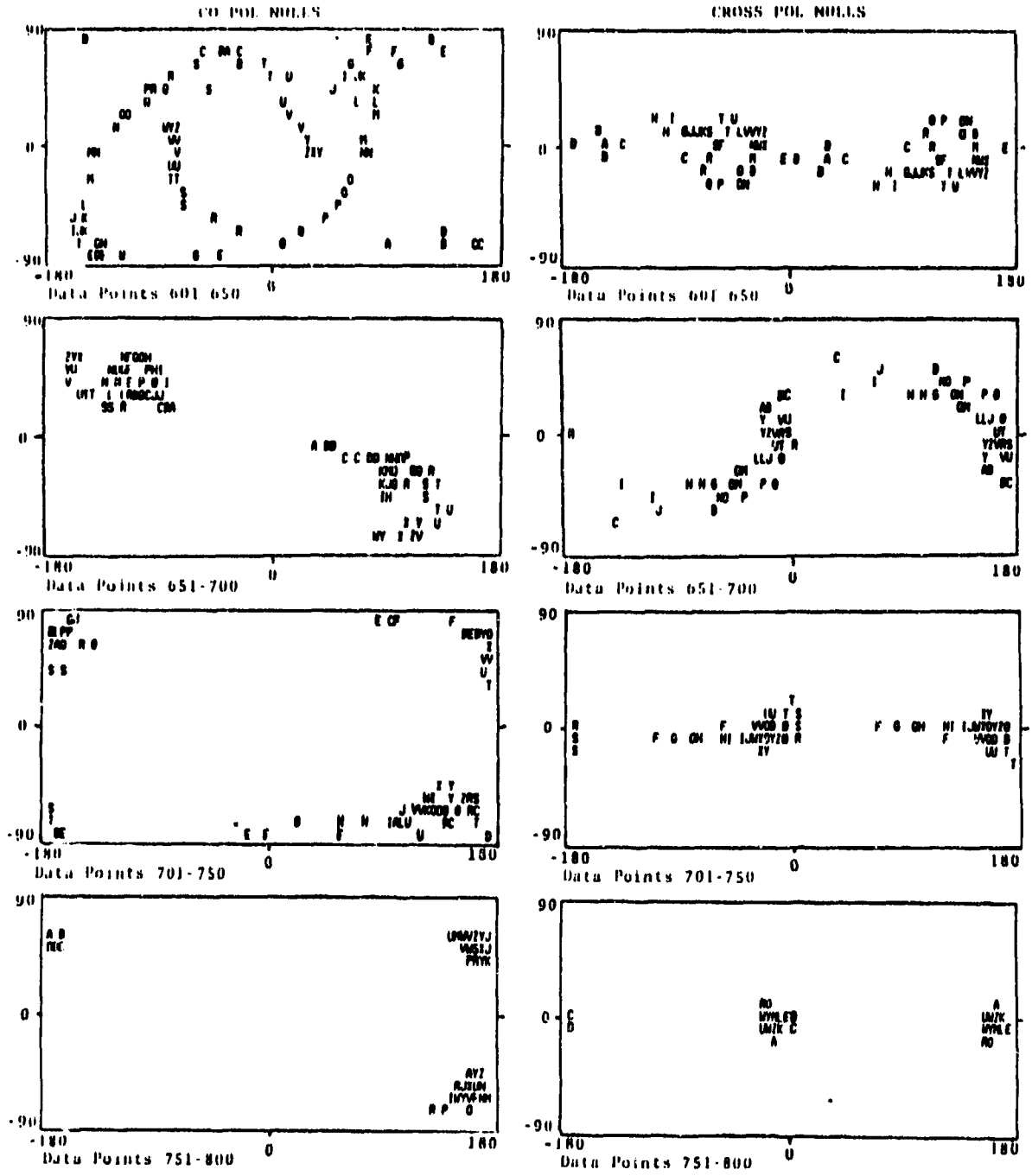

FIGURE 7d - Sportfishing Boat Polarization Nulls
Data Points 601-800

clustering of the cross pol nulls. The copol nulls which tend to cluster in the polar region exhibit considerably more structure than those of the sailboat. An interesting sequence of events is exhibited by the point sequence of 350-600. In the sequence of 350-400 starting with H (Point Number 360 on the amplitude scale) the northern cluster of the copol nulls meanders across the pole down to the equator and back to the pole. The southern cluster remains virtually stationary in the next series of 50 points (401-450). Both copol clusters then start out from the polar region, meander to the equator and move along the equatorial belt in opposite directions, northern cluster to the east and southern to the west with the latter progressing perhaps three times as fast. The next sequences 451-600 traces out the rapid passage of the southern cluster through a counterclockwise spiral and a gradual reformation to the northern and southern clusters. The amplitude information during that sequence of events shows a significant fade of the signal around 450 and a significantly lower $|\sigma_{VV}|$ during the entire sequence of the data points discussed here.

The sportfishing boat displayed the most complex behavior of the polarization nulls as shown in Figures 7b,c, and d. The sequence of points 451-500 exhibits nearly classic example of a flat plate response. All the other copol patterns are very rich in signature information and suitable techniques will need to be developed to permit a meaningful interpretation.

It is very clear from the above illustrations that whereas one could probably recognize the sailboat from the launch or the sportfishing boat by the fading rate of the amplitude signal, separating the launch from the sportfishing boat, would be difficult using amplitude signal alone and in particular only $|\sigma_{HH}|$ which is the usual quantity that is monitored by conventional Navy radars. Although both targets exhibit reasonably similar fading patterns, polarization signatures are distinctly different and if full RCS matrix information is used,

one could quite readily distinguish the launch from the sport-fishing boat simply by observing the behavior of the polarization nulls plotted on the Poincaré Sphere.

3.3 RCS Matrix Measurements of Clutter

For the purpose of illustrating the RCS matrix properties of sea clutter as observed off the Point Loma site, data from four representative samples are shown in Figures 8, 9, 10 and 11. Samples shown represent observations made at elevation angles of 2.9, 3.3, 4.1 and 6.6°. Perusal of the amplitude data shown in part "a" of the above referenced figures reveals quasi periodic fading of $|\sigma_{VV}|$ with periods which appear to depend on the angle of elevation. The longer periods of 75 to 100 milliseconds are associated with the elevation angles of 4.1 and 6.1° and shorter periods of 50 to 75 milliseconds are associated with the elevation angles of 2.9° and 3.3°.

As expected, $|\sigma_{HH}|$ is much weaker than $|\sigma_{VV}|$. It is interesting to note that $|\sigma_{HH}|$ is in general significantly weaker than the cross polarized component $|\sigma_{HV}|$. However, since both $|\sigma_{HH}|$ and $|\sigma_{HV}|$ are fairly close to the receiver noise level and inasmuch as this data represents preliminary observations, these results should be treated as being more qualitative than quantitative until additional data become available.

Observed polarization properties of the clutter shown in parts b, c, and d of Figures 8, 9, 10 and 11 are in general agreement with earlier observations based on the Four Frequency Radar NRL data. However, they do exhibit a fair amount of fine structure which was not observed in the NRL data.

Whenever the signal is strong, as during the peak of the fading cycle, the clustering of the polarization nulls is

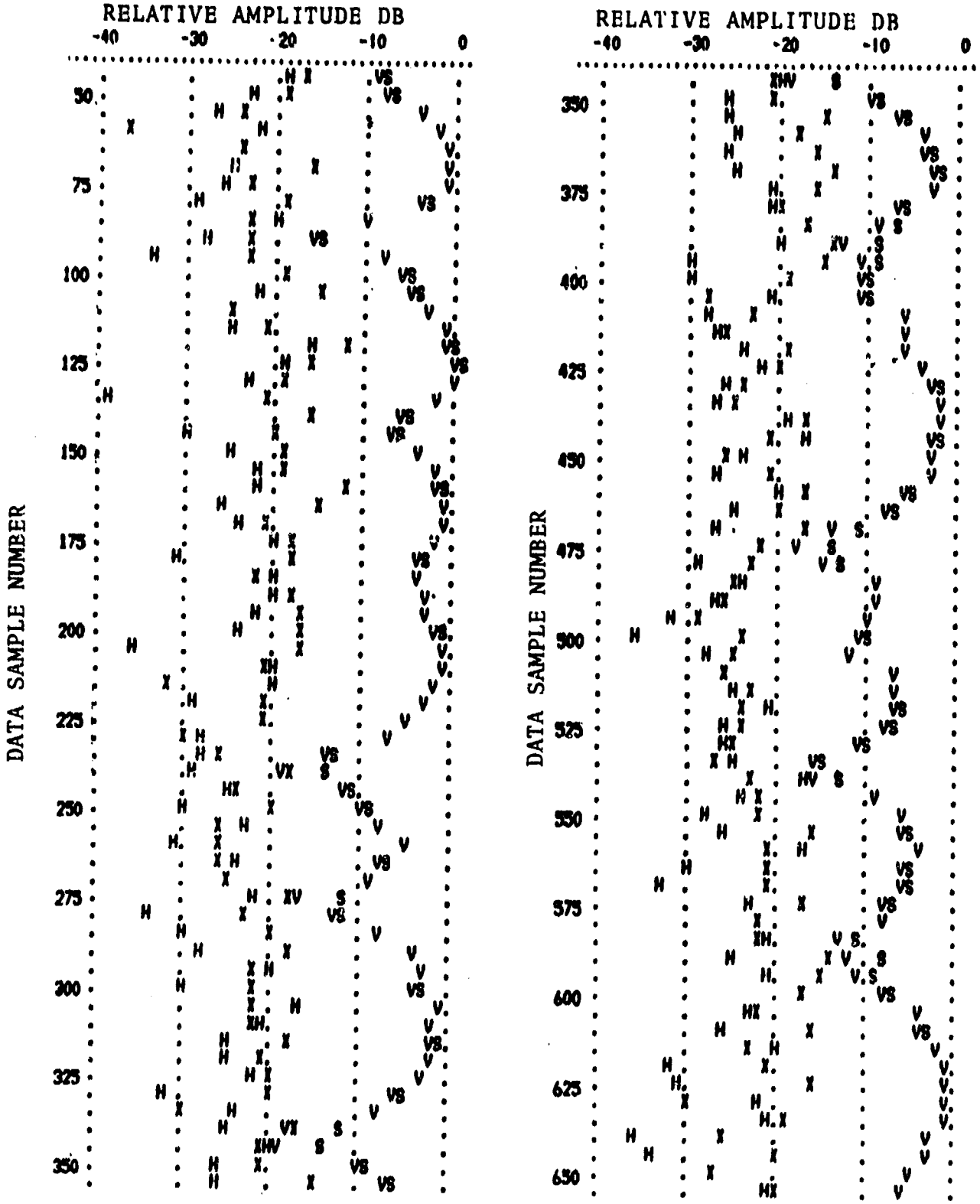

FIGURE 8a - Clutter Amplitude; Angle of Elevation = 2.9

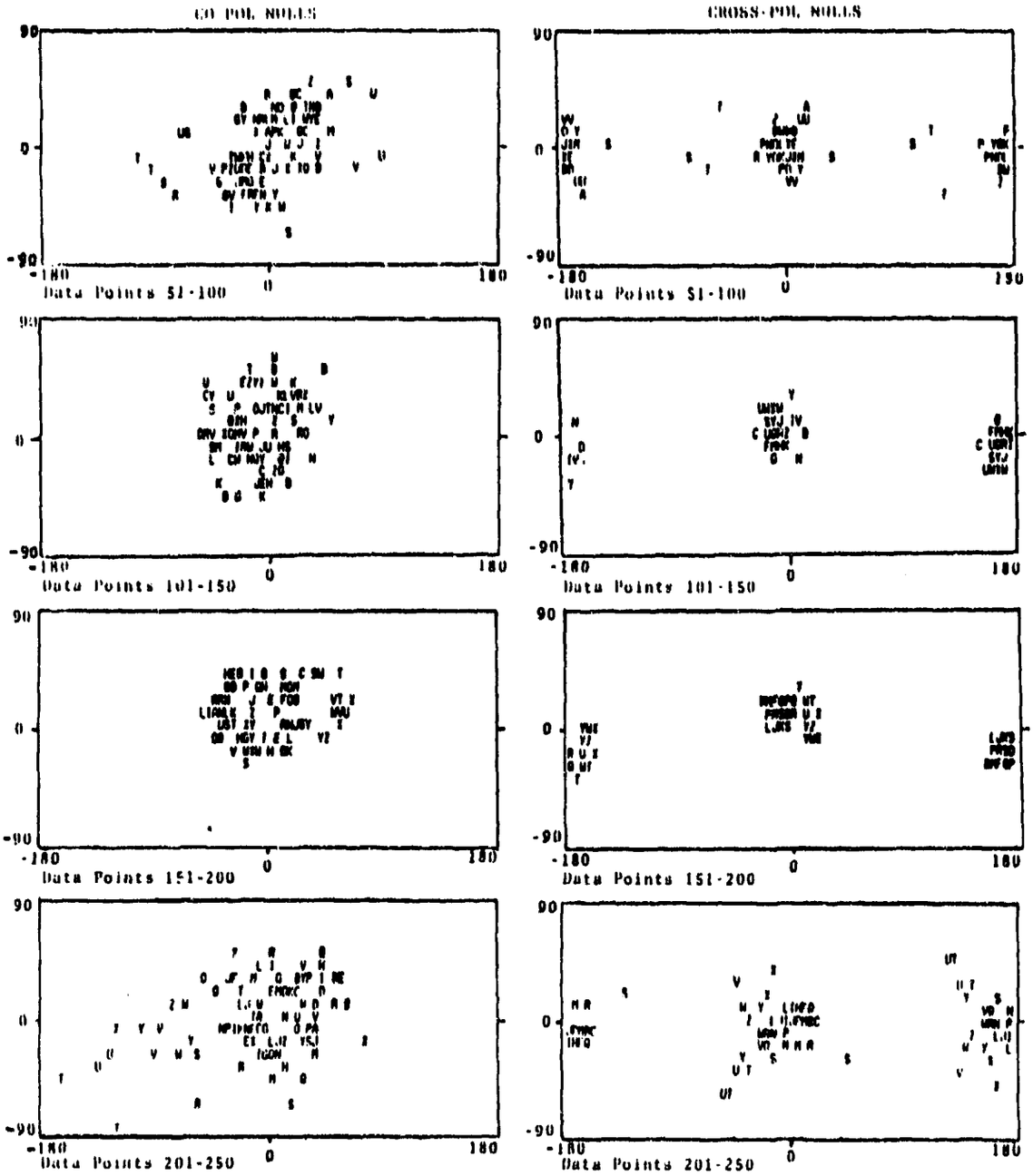

FIGURE 8b - Clutter Polarization Nulls
Elevation Angle = 2.9
Data Points 51-250

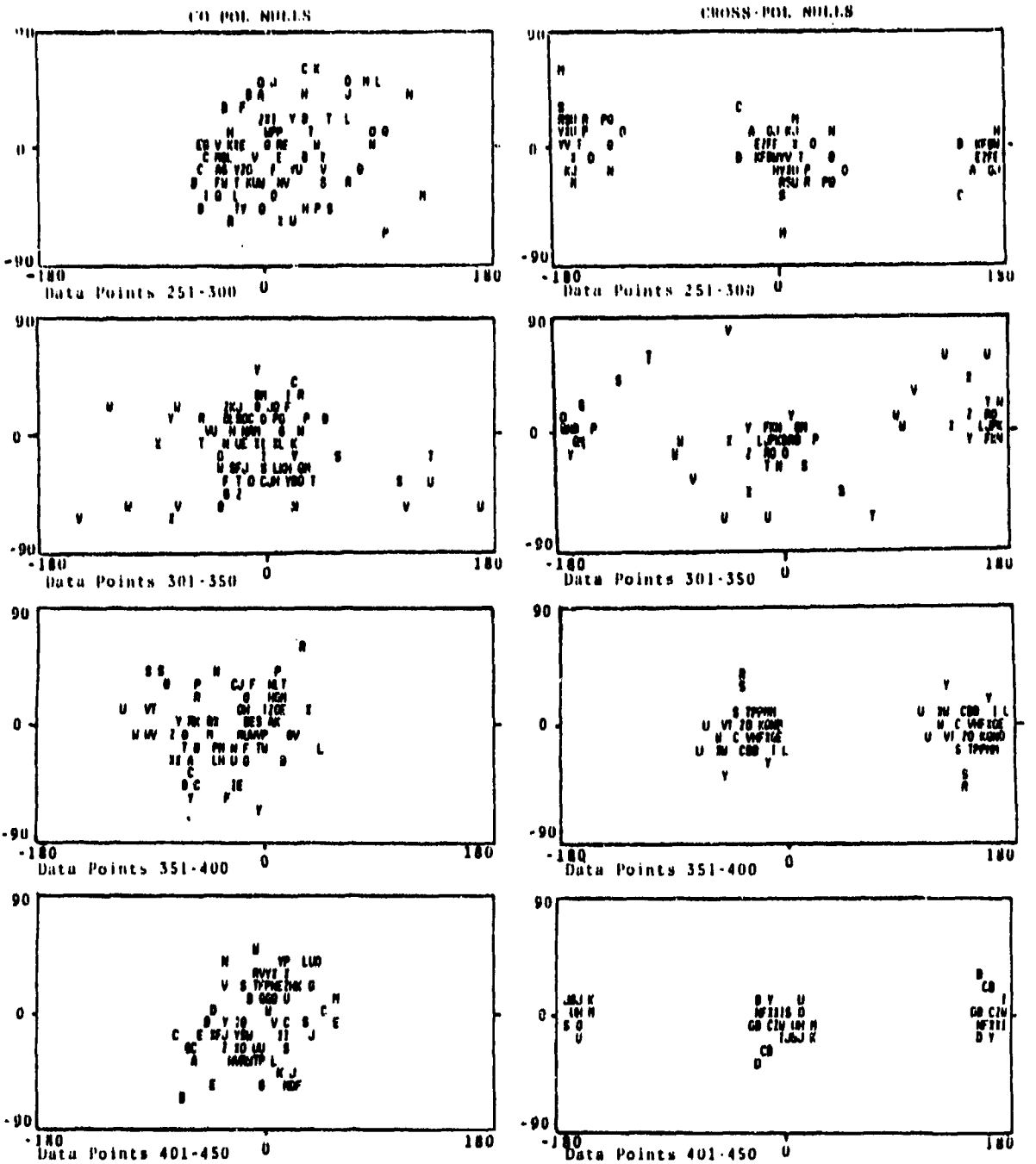

FIGURE 8c - Clutter Polarization Nulls
Elevation Angle = 2.9
Data Points 251-450

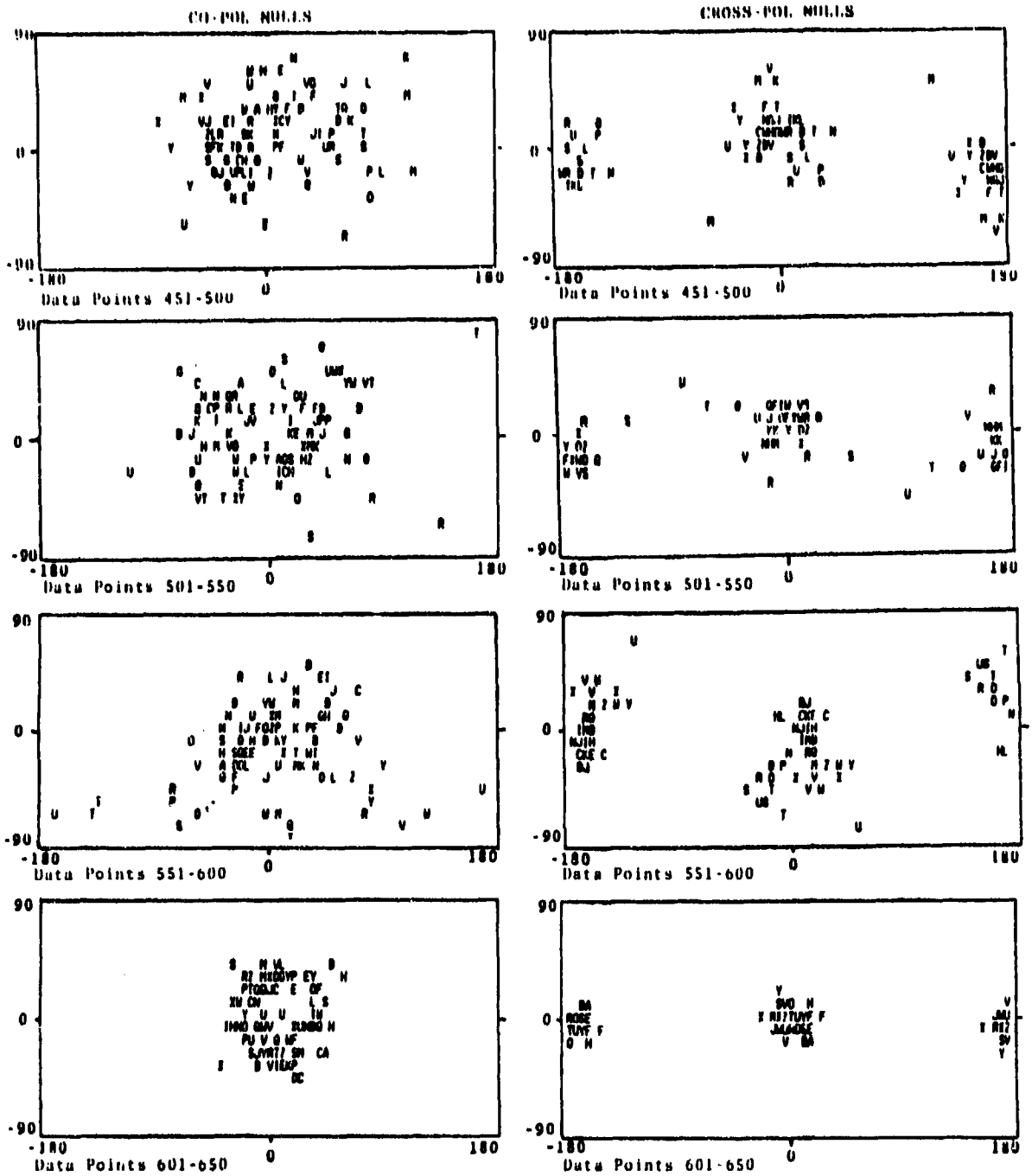

FIGURE 8d - Clutter Polarization Nulls
Elevation Angle = 2.9
Data Points 451-650

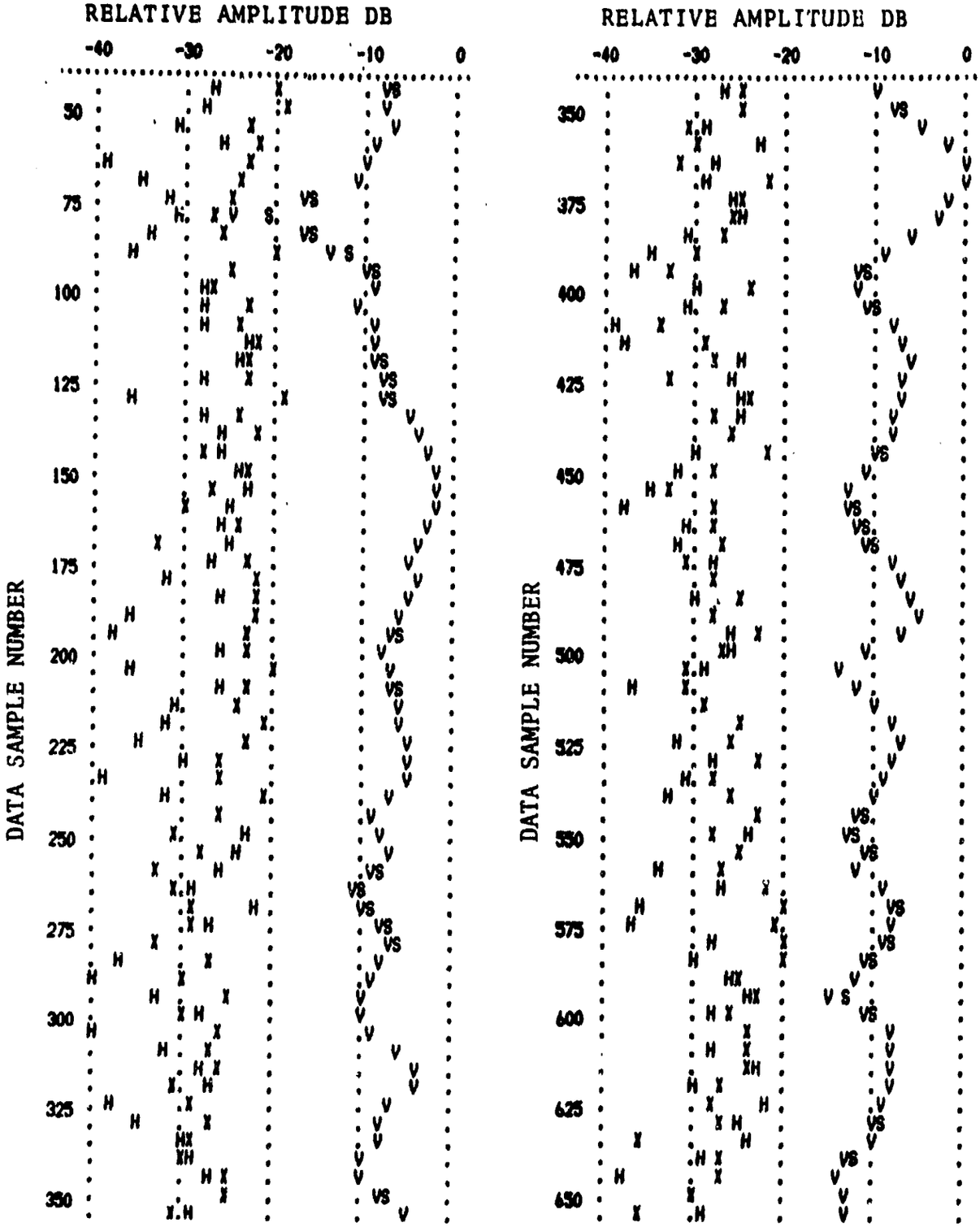

FIGURE 9a - Clutter Amplitude; Angle of Elevation = 3.3

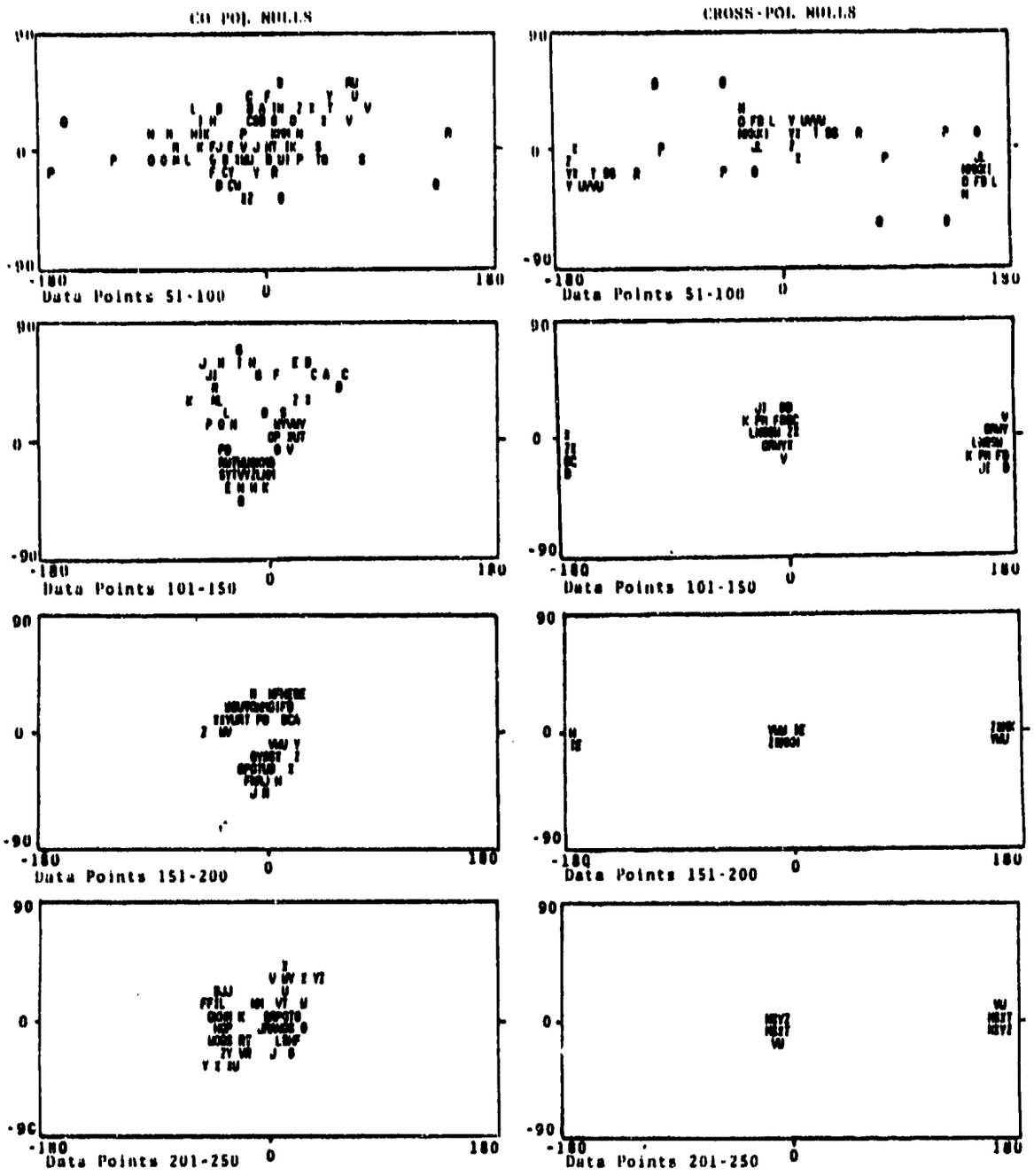

FIGURE 9b - Clutter Polarization Nulls
Elevation Angle = 3.3
Data Points 51-250

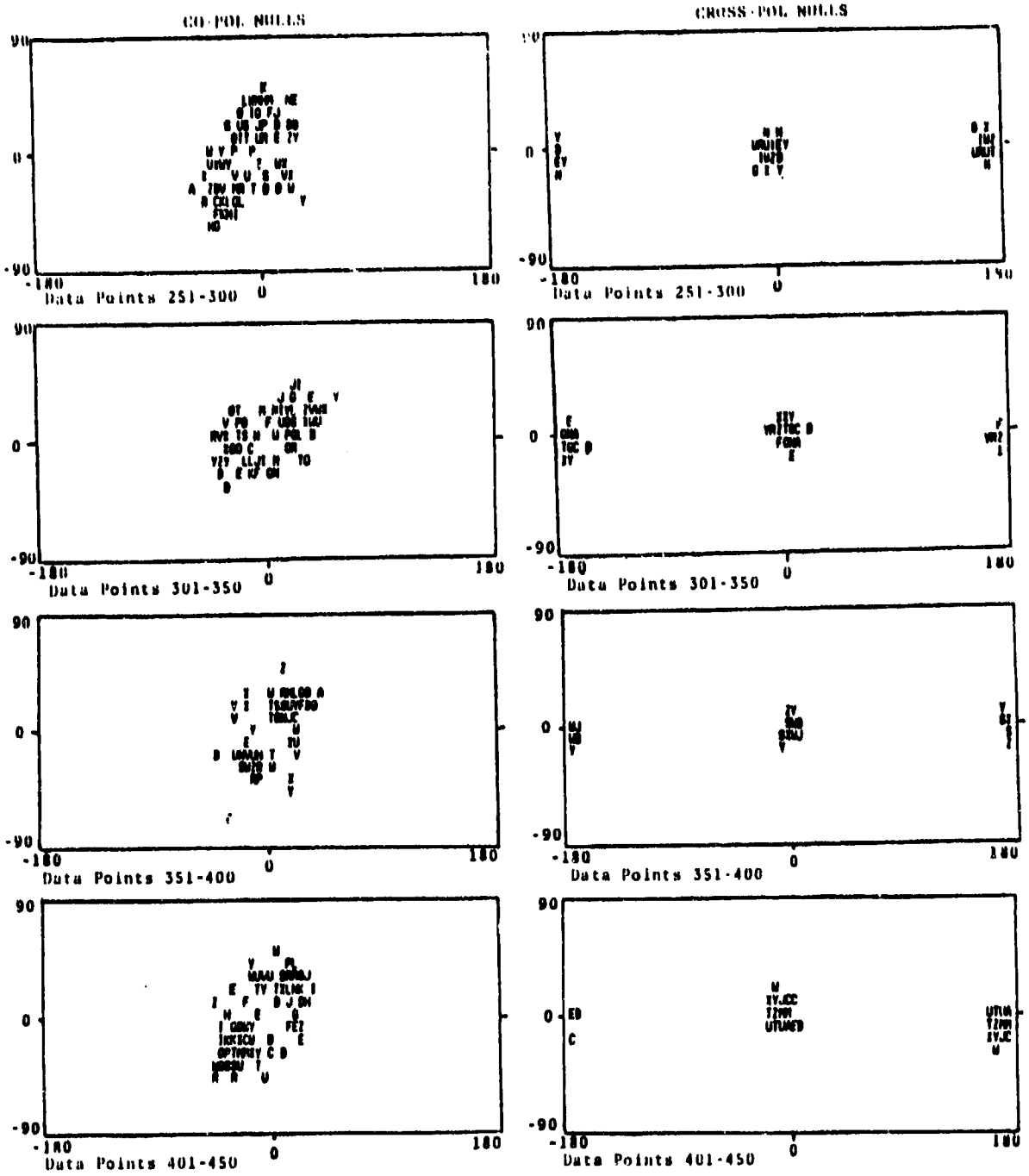

FIGURE 9c - Clutter Polarization Nulls
Elevation Angle = 3.3
Data Points 251-450

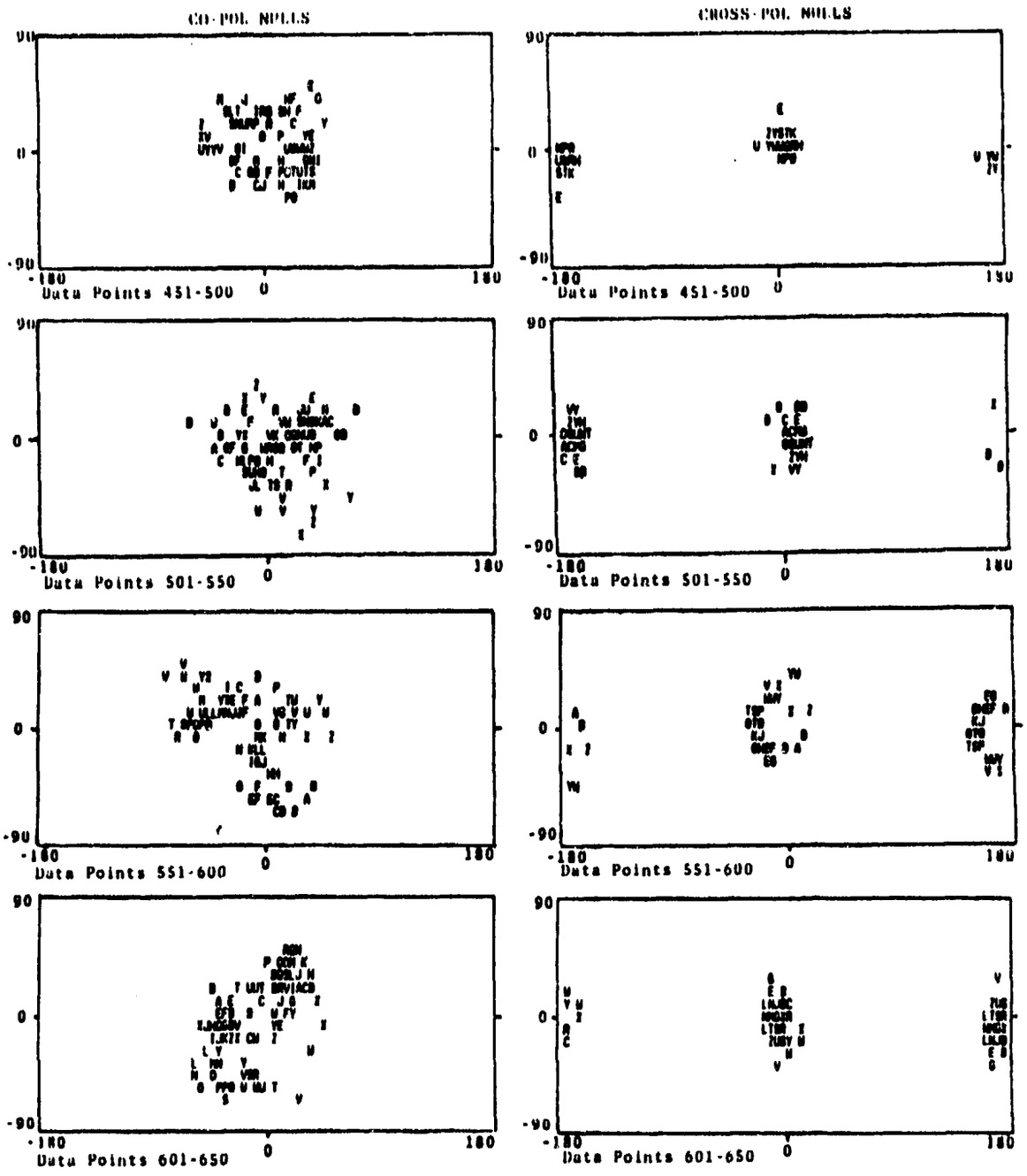

FIGURE 9d - Clutter Polarization Nulls
Elevation Angle = 3 3
Data Points 451-650

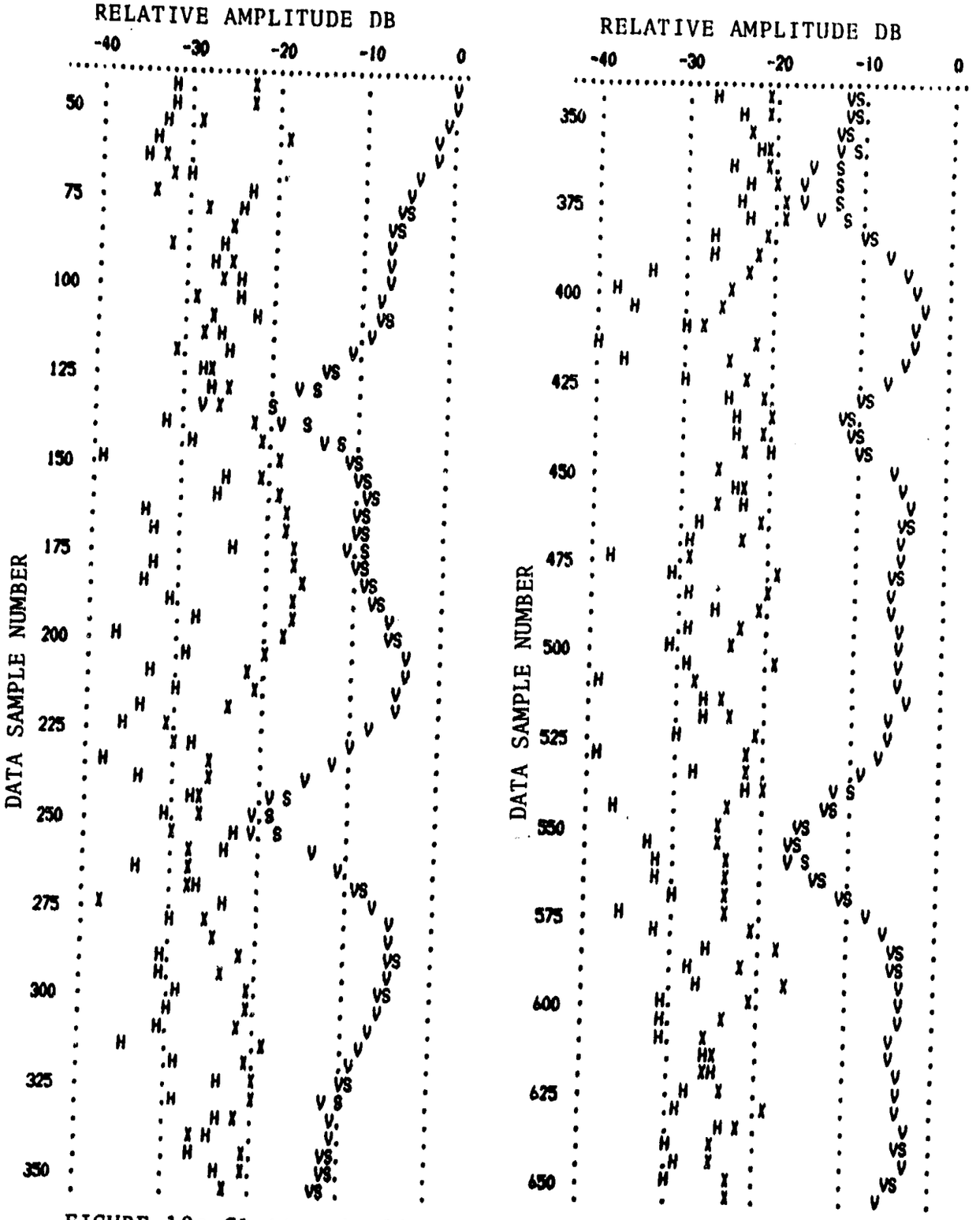

FIGURE 10a-Clutter Amplitude; Angle of Elevation = 4.1

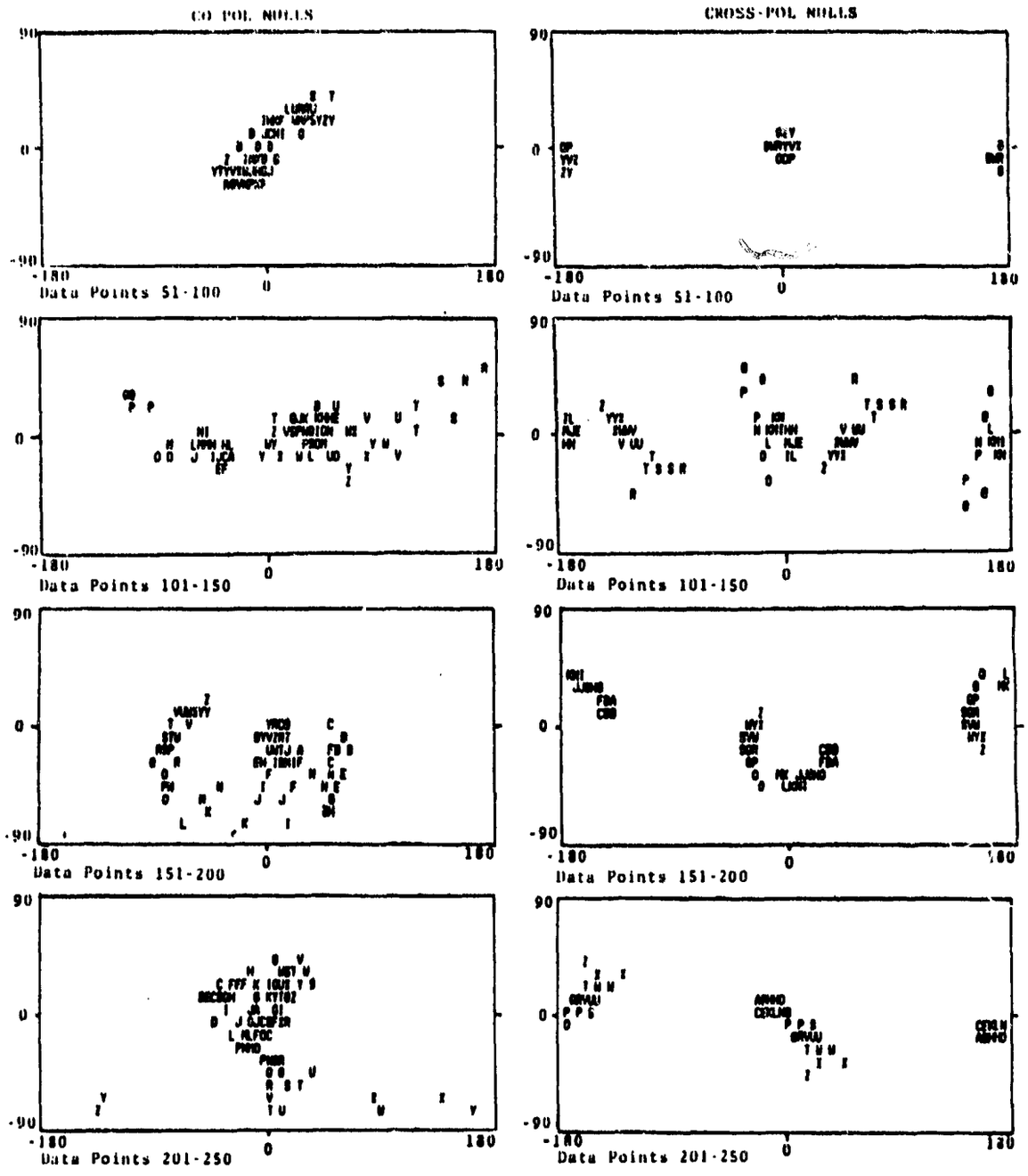

FIGURE 10b - Clutter Polarization Nulls
Elevation Angle = 4.1
Data Points 51-250

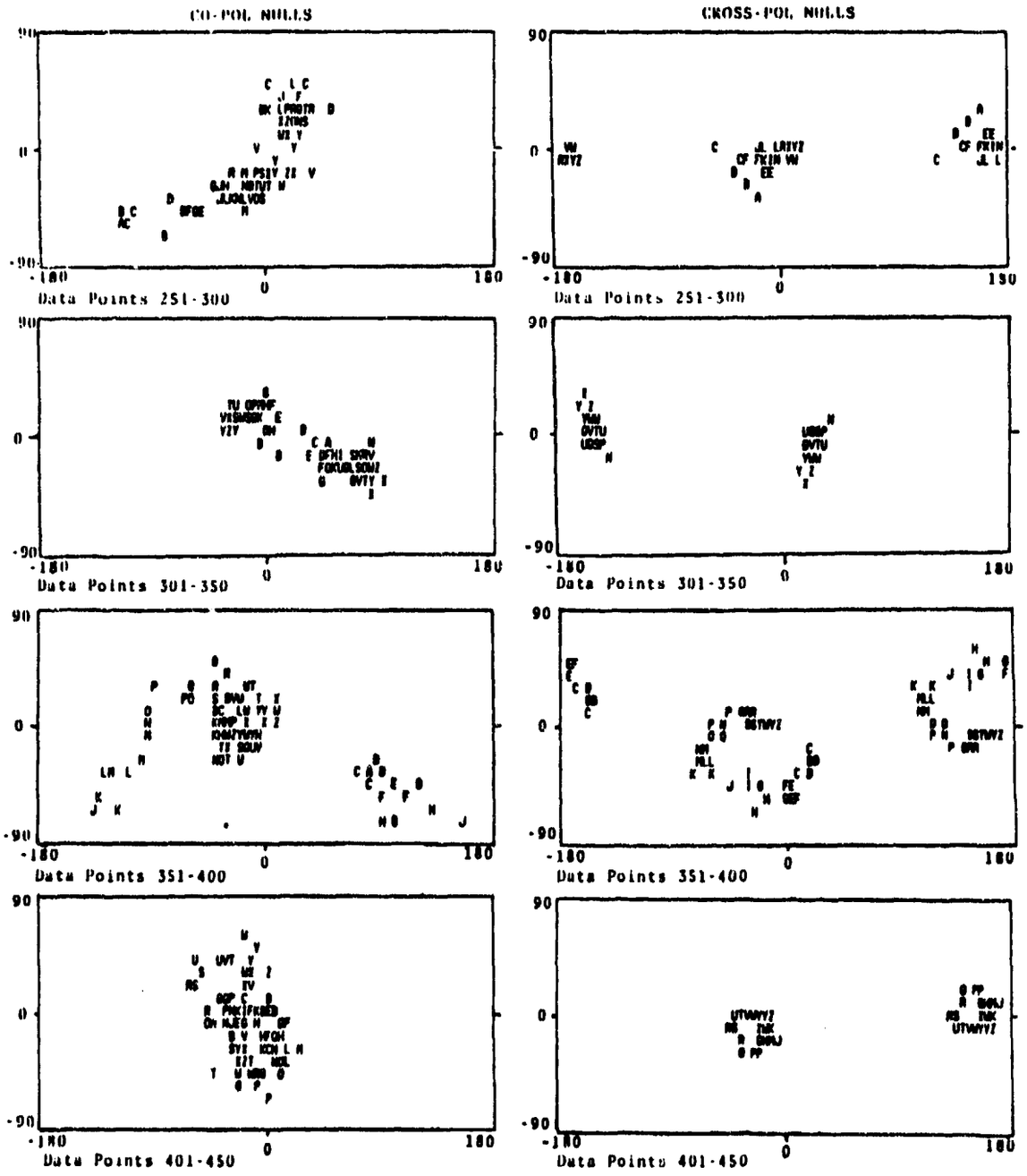

FIGURE 10c - Clutter Polarization Nulls
Elevation Angle = 4.1
Data Points 251-450

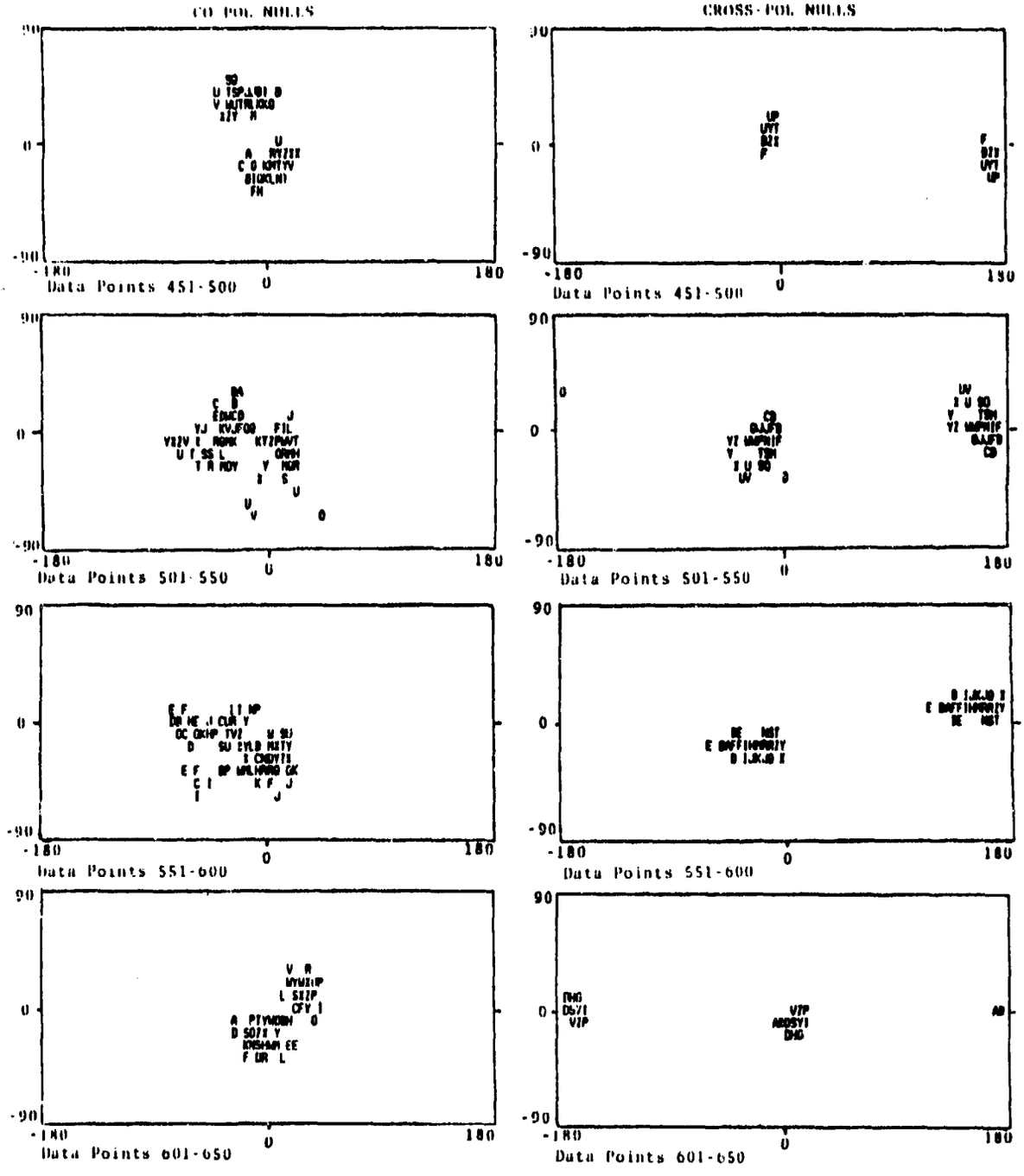

FIGURE 10d - Clutter Polarization Nulls
Elevation Angle = 4.1
Data Points 451-650

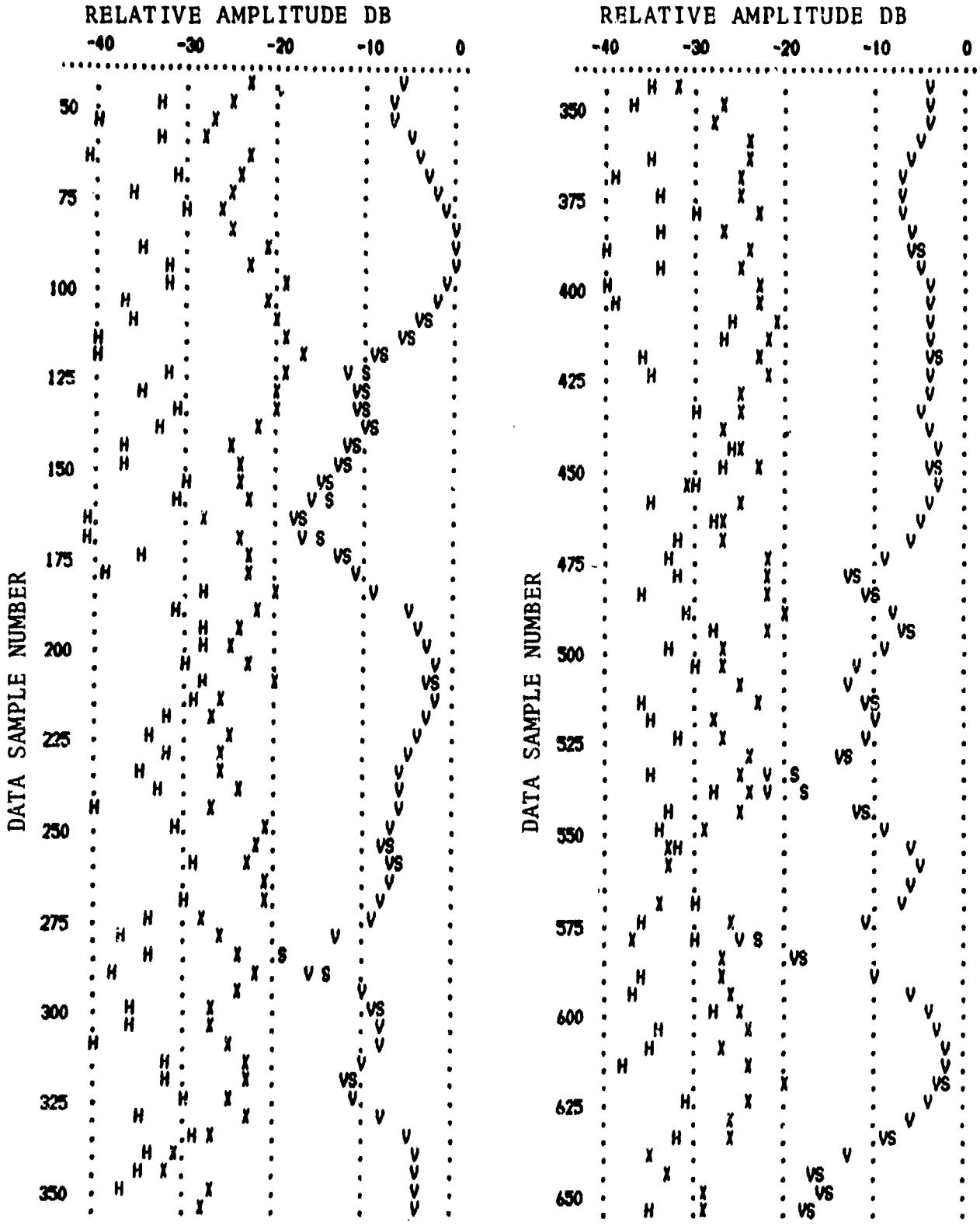

FIGURE 11a-Clutter Amplitude; Angle of Elevation = 6.1

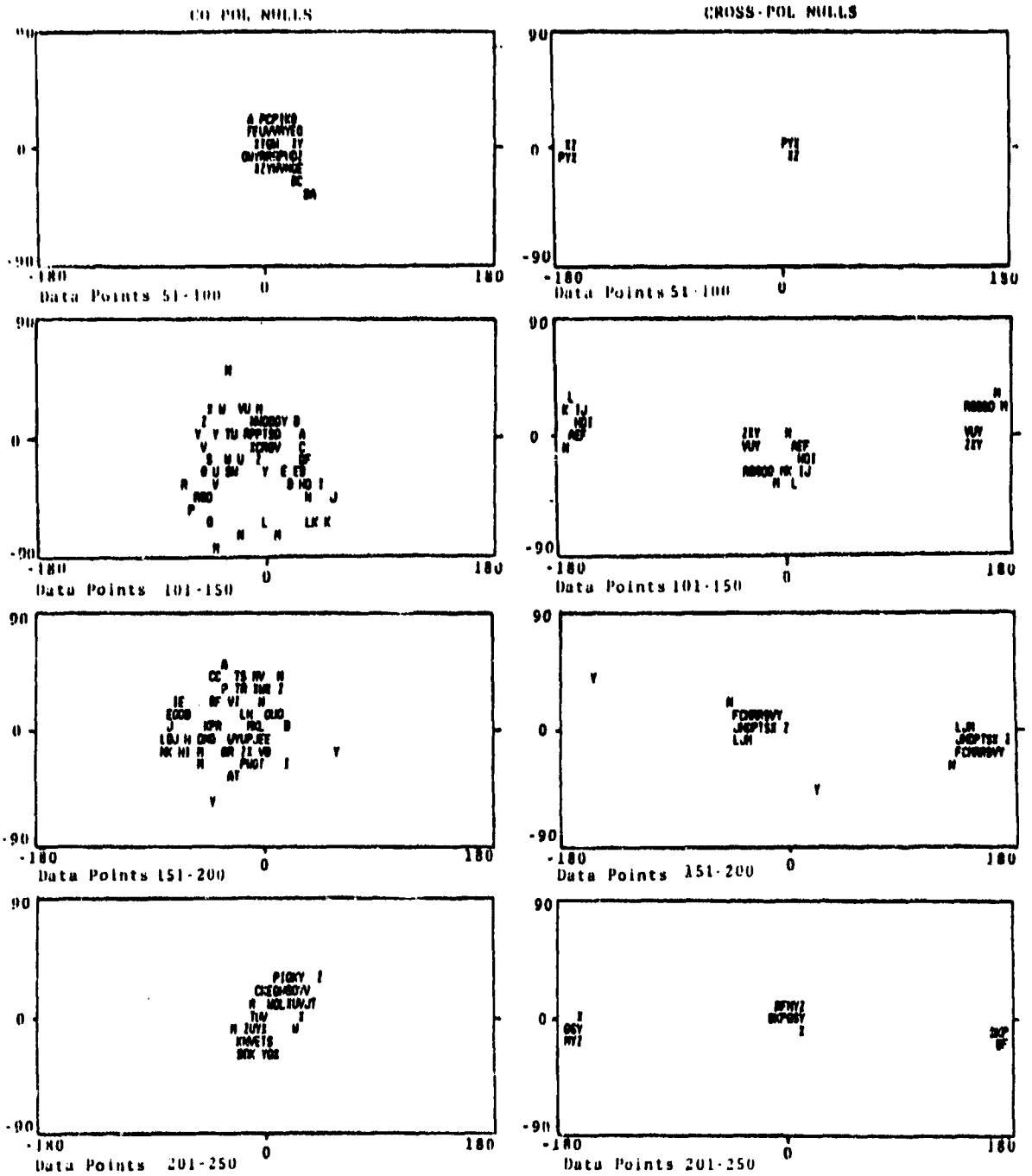

FIGURE 11b - Clutter Polarization Nulls
Elevation Angle = 6.1
Data Points 51-250

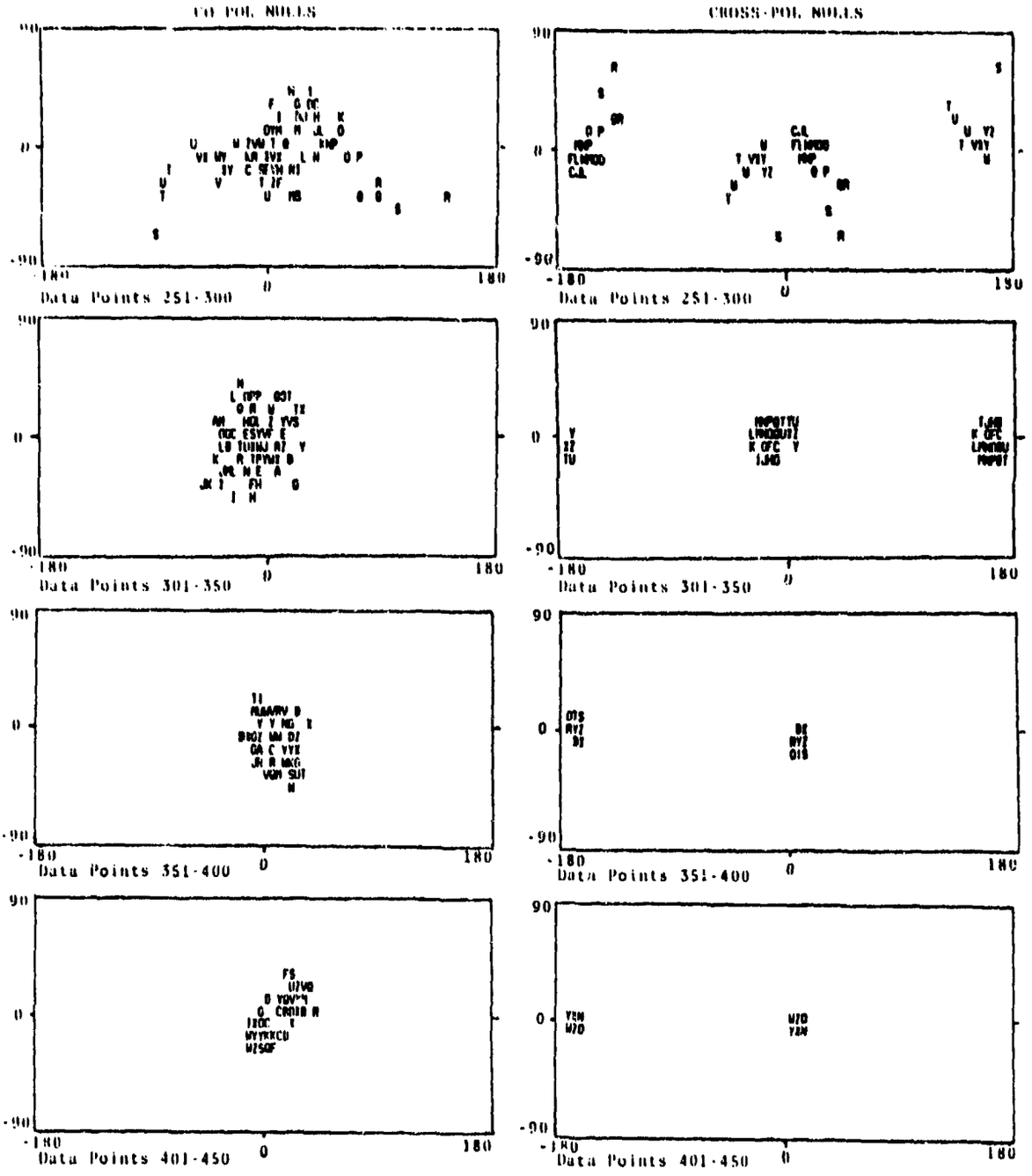

FIGURE 11c - Clutter Polarization Nulls
Elevation Angle = 6.1
Data Points 251-450

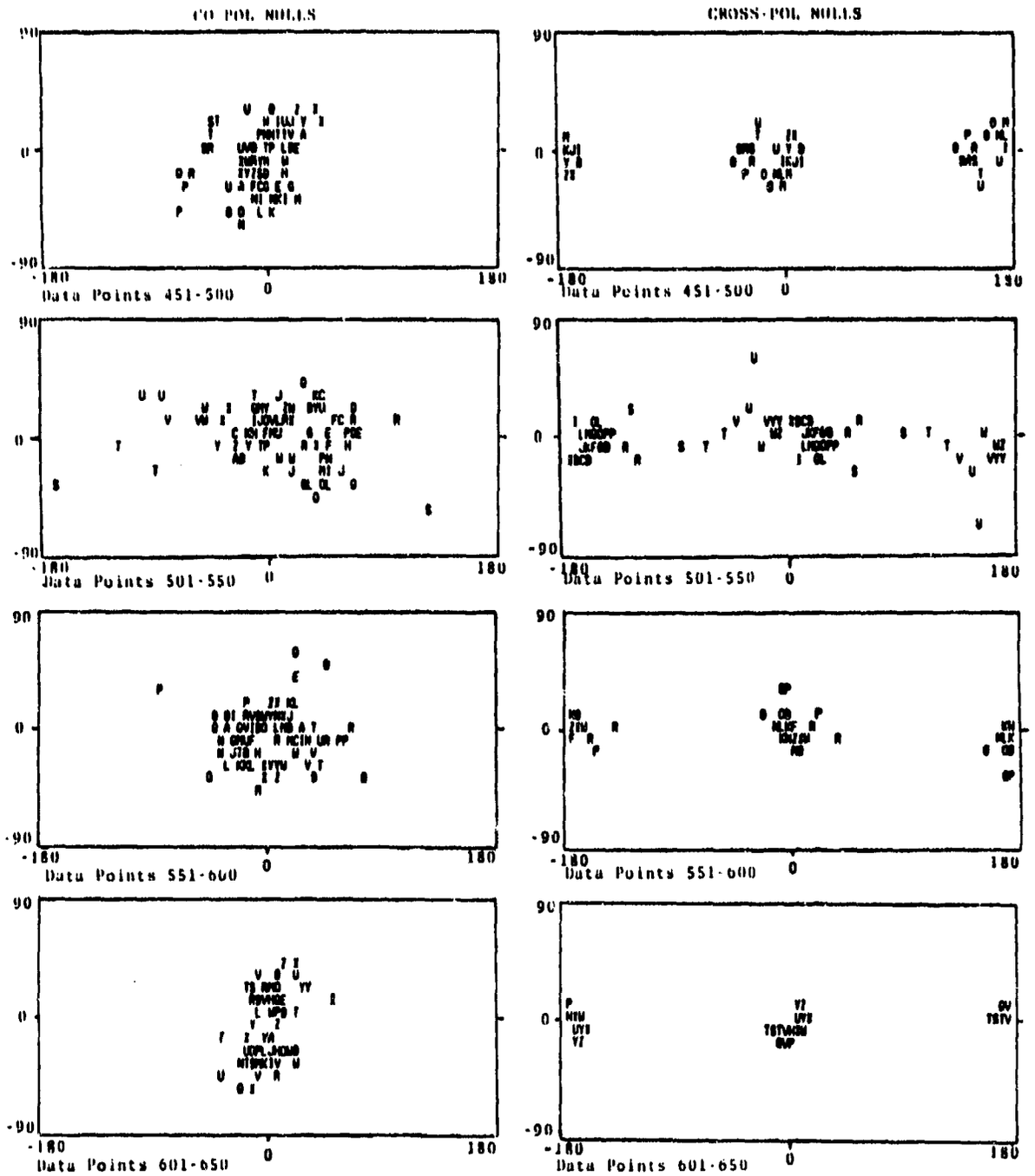

FIGURE 11d - Clutter Polarization Nulls
Elevation Angle = 6.1
Data Points 451-650

well defined. As the signal fades the clustering becomes less defined. This is probably caused by low signal to noise ratio. There seems to be some evidence that the two copol clusters interchange their positions. This is suggested by co pol patterns in Figure 10b.

3.4 Clutter to Noise Ratio

The measured clutter to noise ratio as a function of range for a calm sea state (estimated between sea states 1 and 2) is plotted in Figure 12. Also shown in this figure are theoretical curves for sea state 3 based upon the computed* values of sea clutter cross section given in Table II, the system parameters contained in Table I, and a receiver noise level of -98 dBm.

The measured data is considerably lower than the computed curves which is not surprising in view of the lower sea state which prevailed throughout these measurements. Empirically derived relationships** predict a 10 - 15 dB decrease in the VV clutter level between sea state 3 (8 knot wind) and sea state 1 (2 knot wind).

Less expected are the amount that the VV return exceeds the other two components (greater than 10 dB) and the fact that the cross polarized component is larger than the HH component. These effects are thought to be real since the data taken on targets of opportunity during the same period do not suggest any imbalance between channels. Furthermore, the actual measurements were performed with ±45 degree linear polarization which was converted to vertical and horizontal in the data processing. Thus, any equipment errors would probably be reflected in both VV and HH components equally.

---

* Normalized clutter cross sections were computed by Mr. John Daley of NRL.

**Daley, John, "An Empirical Sea Clutter Model", Naval Research Laboratory, NRL Memorandum Report 2668, Oct. 1973.

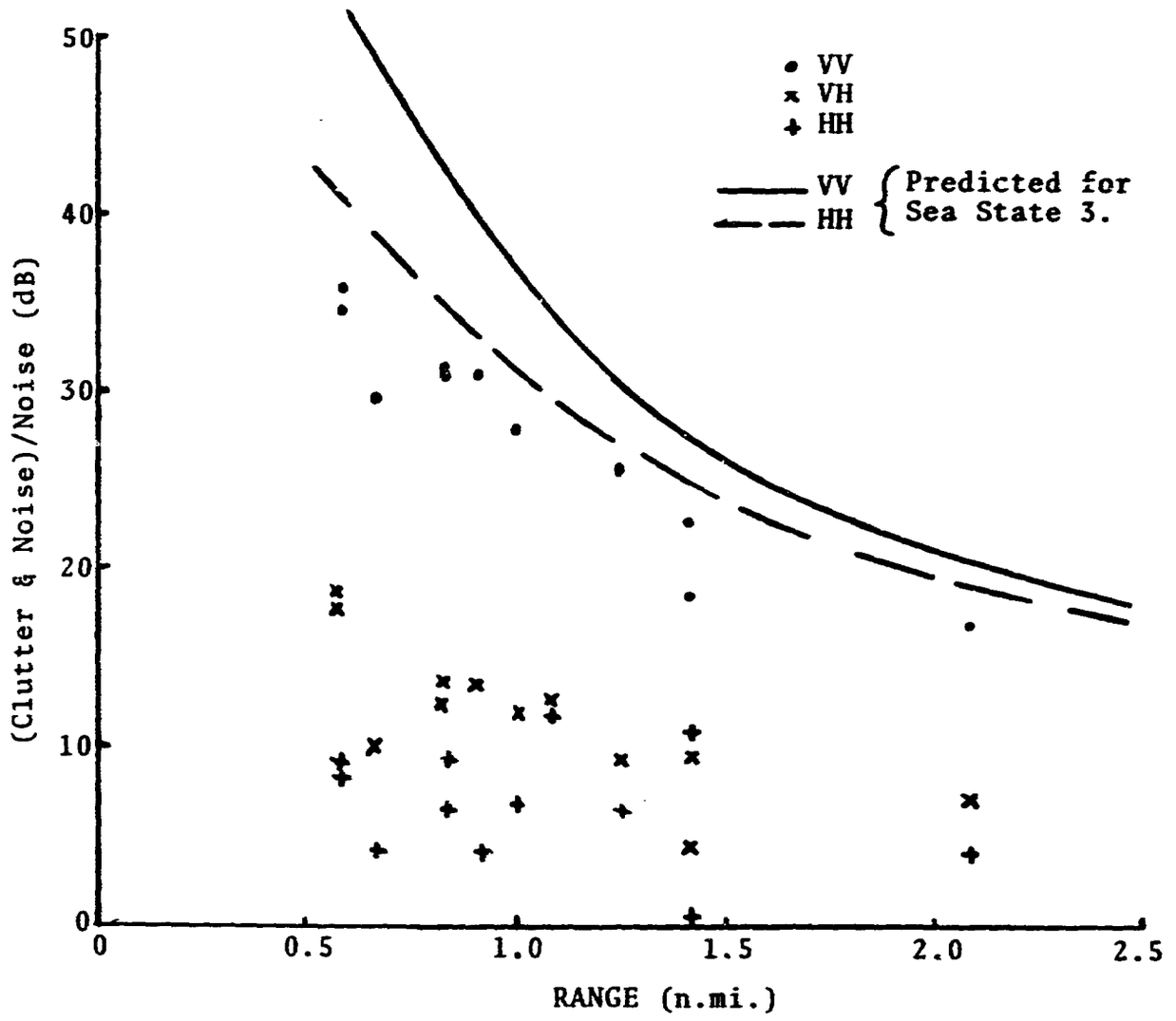

FIGURE 12: Clutter to Noise Ratio as a function of Range.

TABLE II

EXPECTED CLUTTER VALUES FOR SEA STATE 3

Range (n.mi.)	Incidence Angle (Degrees)	Normalized Clutter Cross Section (dB)			Expected Received Power (dBm)		
		VV	HH	VH	VV	HH	VH
0.5	7.50	-31	-43	-45	-43	-55	-57
0.8	4.70	-33	-45	-47	-51	-63	-65
1.0	3.77	-40	-46	-48	-61	-67	-69
2.0	1.89	-47	-48	-50	-77	-78	-80
3.0	1.26	-49	-49	-51	-84	-84	-86
4.0	0.94	-50	-50	-52	-89	-89	-91

3.5 Applicability to Target Classification

Although the data shown here is fragmentary, it clearly illustrates the richness of polarization signatures. Given the limited set of radar returns discussed here, it is easy to identify which set of RCS matrix data goes with clutter, sailboat, launch and the sportfishing boat.

It is obviously not possible at this point in time, to assess the full potential of this technique to accomplish all the objectives of the target classification problem but it is very reasonable to conjecture that as the library of RCS matrix signatures is acquired on a variety of targets and the familiarity with this technique is increased, the RCS matrix technique will very substantially augment the Navy capabilities to detect and classify radar targets.

4.0 CONCLUSIONS AND RECOMMENDATIONS

An experimental facility to study RCS matrix properties of sea clutter and of radar targets in sea clutter has been instrumented. Preliminary data on clutter and on targets of opportunity has been collected and examined.

It is quite apparent from the examination of these preliminary results that the RCS matrix technique can provide rich RCS signatures which should significantly augment Navy radar capabilities to improve target detectability and target classification.

In spite of the demonstrated potential, the RCS matrix technique will need a carefully planned development. It is therefore recommended that the next phases of the effort be oriented toward the acquisition of a meaningful data base of the RCS matrix signatures of targets of interest. As soon as some of this data base becomes available, a systematic investigation should be initiated for the development of suitable algorithms which would be able to categorize RCS matrix signatures in a manner which would be efficient in achieving target classification.

APPENDIX A

RADAR CROSS SECTION MATRIX

The following is a brief review of the basic concepts involved in the Radar Cross Section (RCS) Matrix. This technique allows a complete description of radar target reflectivity in terms of the intrinsic properties of the target without reference to the polarization properties of the measuring radar. Polarization ellipses are represented as points on the Poincaré Sphere or Polarization space. Transformation equations are given at the end of this Appendix.

The RCS matrix is formed by alternately illuminating the target with two orthogonal polarizations and coherently recording the co- and cross-polarized responses.* Since any polarization can be expressed as a linear combination of any set of orthogonal polarizations, it follows from the Superposition Theorem that the information contained in the RCS matrix is adequate to describe the response of the target to any arbitrary polarization. In other words, the RCS matrix parameters measured in one set of orthogonal polarizations can be transformed to any number of RCS matrices which would have been obtained with other orthogonal sets of polarizations. This is illustrated in Figure 1.

It should be noted that in the most general way the RCS matrix is an eight-dimensional quantity (four complex numbers). However, the Reciprocity Theorem requires that $\sigma_{ij} = \sigma_{ji}$ and since phases are relative, one of the phases can be set to zero, and the RCS matrix reduces to a five-dimensional quantity.

---

*This technique does not require orthogonal polarizations. In practical situations it is usually much easier to use an approximately orthogonal pair of polarizations and then have the computer orthogonize the data through the use of a priori calibration obtained by measuring the response of standard targets such as plates and dihedral reflectors whose RCS matrices are accurately known.

RCS MATRIX

$$\begin{vmatrix} \sigma_{HH} & \sigma_{HV} \\ \sigma_{VH} & \sigma_{VV} \end{vmatrix} \longrightarrow \begin{vmatrix} \sigma_{ii} & \sigma_{ij} \\ \sigma_{ji} & \sigma_{jj} \end{vmatrix}$$

FOR ARBITRARY POLARIZATION SET TRANSFORMS TO

DATA — COMPUTED

POLARIZATION GIVING	$\sigma_{ii} = 0$	DEFINES COPOL NULL
POLARIZATION GIVING	$\sigma_{ij} = 0$	DEFINES XPOL NULL

INVARIANTS:

$\sigma_{ij} = \sigma_{ji}$; $\sum_i \sum_j |\sigma_{ij}|^2$; DETERMINANT

TELEDYNE MICRONETICS

FIGURE 1

In general, dealing with a five-dimensional space is difficult. However, it is possible to uniquely represent the RCS matrix as two points on a surface of a sphere. The two latitudes and the two longitudes which account for four out of five dimensions define the polarization properties of the target. The fifth dimension, the radius of the sphere, is the measure of target reflectivity. This is done as follows: Using formal tools of matrix algebra we seek out transformations which result in the RCS matrix whose element $\sigma_{ij} = 0$. Since such transformation involves a quadratic equation we get, in general, two solutions each representing a polarization which, had it been used by the radar, would have resulted in zero energy in the co-polarized return. We call this polarization "CO-POL" null. To represent the polarizations graphically we resort to the Poincaré Sphere where every possible polarization is uniquely mapped as a point on the surface of the sphere. Major properties of the Poincaré Sphere are listed in Figure 2.

The two co-polarized nulls represent the polarization properties of the radar target. The conservation of energy requires that the sum of the reflected energies as given by the sum of the squares of the absolute values of the RCS matrix elements be invariant under matrix transformation. The square root of this sum can be used as the radius of the Poincaré Sphere to describe target reflectivity.

In addition to the co-polarized nulls, we can also find the cross-polarized or cross-pol nulls by specifying that the transformed RCS matrix be a diagonal matrix, i.e., $\sigma_{ij} = \sigma_{ji} = 0$. Physically this means that if the target is illuminated with the polarization i or j all return will be co-polarized.

There is no new information provided by this transformation since the solution for the co-pol nulls used up all of the five dimensions contained in the original RCS matrix.

REPRESENTATION OF POLARIZATION BY POINCARÉ SPHERE

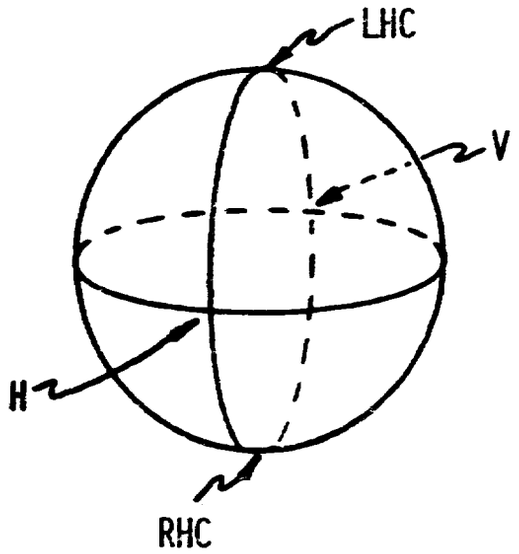

EACH POINT ON THE SURFACE UNIQUELY SPECIFIES A POLARIZATION ELLIPSE.
AXIAL RATIO DETERMINES LATITUDE.
TILT ANGLE DETERMINES LONGITUDE.
SENSE OF ROTATION DETERMINES HEMISPHERE.

PROPERTIES OF POINCARÉ SPHERE

1. EACH POLARIZATION ELLIPSE OCCUPIES A UNIQUE POINT.
2. UPPER HEMISPHERE REPRESENTS ALL LEFT-HANDED POLARIZATIONS.
3. NORTH POLE REPRESENTS LEFT-HANDED CIRCULAR POLARIZATION.
4. ALL LINEAR POLARIZATIONS LIE ON THE EQUATOR.
5. ORTHOGONAL POLARIZATIONS OCCUPY ANTIPODAL POINTS.
6. RANDOM POLARIZATIONS ARE UNIFORMLY DISTRIBUTED.

TELEDYNE MICRONETICS

FIGURE 2

The two cross-pol nulls (which by the requirements of the Reciprocity Theorem are orthogonal) bisect the two segments of the great circle path on the Poincaré Sphere defined by the two co-pol nulls. This is illustrated in Figure 3. In several physical phenomena, such as the sea clutter, cross-pol nulls tend to cluster in well defined regions and frequently help to provide physical insight which would not be quite as apparent from the examination of co-pol nulls alone.

PROPERTIES OF POLARIZATION NULLS

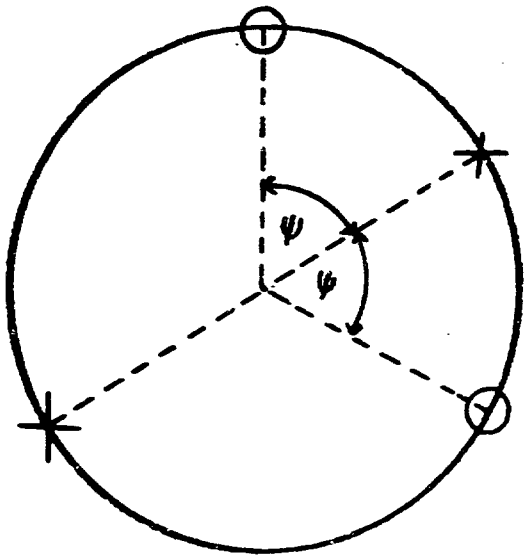

1. THE TWO COPOL AND THE XPOL NULLS LIE ON THE SAME GREAT CIRCLE PATH ON THE POINCARÉ SPHERE.
2. XPOL NULLS ARE ORTHOGONAL AND BISECT THE ANGLE BETWEEN THE COPOL NULLS.
3. TWO COPOL OR ONE COPOL AND ONE XPOL NULL UNIQUELY DEFINE THE POLARIZATION PROPERTIES OF THE RCS MATRIX.

NOTE: THE TWO LATITUDES AND THE TWO LONGITUDES OF THE TWO POINTS (TWO COPOL OR ONE COPOL AND ONE XPOL) REPRESENT FOUR OF THE FIVE DIMENSIONS OF THE RCS MATRIX. THE FIFTH DIMENSION WHICH IS THE RADIUS, REPRESENTS TARGET REFLECTIVITY AND IS GIVEN BY

$$R^2 = \sum_{i=1}^{2} \sum_{j=1}^{2} |\sigma_{ij}|^2$$

WHICH IS AN INVARIANT IN THE RCS MATRIX TRANSFORMATIONS.

TELEDYNE MICRONETICS

FIGURE 3

TRANSFORMATION EQUATIONS FOR POINCARÉ SPHERE

If an arbitrarily polarized signal is expressed as a sum of right and left (R and L) circularly polarized components or as a sum of horizontally and vertically polarized components (H and V) where R, L, H and V are complex amplitudes and ρ, θ, ϕ are the polar coordinates of the Poincaré Sphere then the following relationships apply:

$$R = (H+jV)/\sqrt{2}$$
$$L = (H-jV)/\sqrt{2}$$
$$H = (R+L)/\sqrt{2}$$
$$jV = (R-L)/\sqrt{2}$$

$$\rho^2 = |L|^2+|R|^2 = |H|^2+|V|^2$$

Axial Ratio = $\tan(\pi/4+\theta/2)$

Tilt angle of the ellipse = $\phi/2$

$$R/L = \tan\theta/2 \exp(j\phi) \qquad 0 \leq\theta\leq\pi$$
$$V/H = \tan\psi/2 \exp(j\beta) \qquad 0 \leq\psi\leq\pi$$

where

$$\cos\psi = \sin\theta\cos\phi$$
$$\tan\beta = \cos\theta/(\sin\theta\sin\phi)$$
$$\cos\theta = \sin\psi\sin\beta$$
$$\tan\phi = \sin\psi\cos\beta/\cos\psi$$

The correct quadrant for β or ϕ is determined in the usual way by signs of the numerator and the denominator of the tangent function.

Poincaré Sphere Convention:

Left circular polarization is at the north pole.
Horizontal polarization is at 0° longitude on the equator.